AD-A170 329 TRIAXIAL TESTING OF FIRST-YEAR SEA ICE(U) COLD REGIONS 1/1
RESEARCH AND ENGINEERING LAB HANOVER NH
J A RICHTER-MENGE ET AL. DEC 86 CRREL-86-16

UNCLASSIFIED F/G 8/12 NL

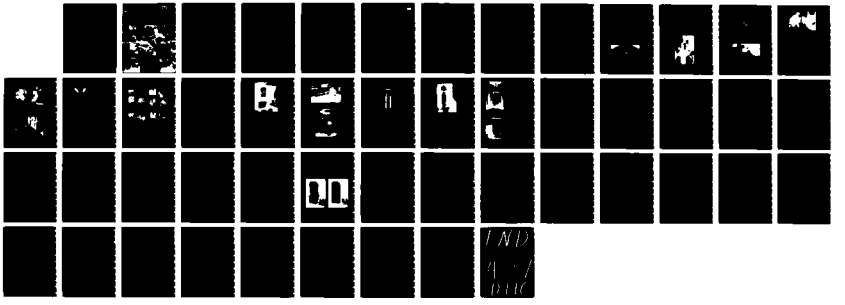

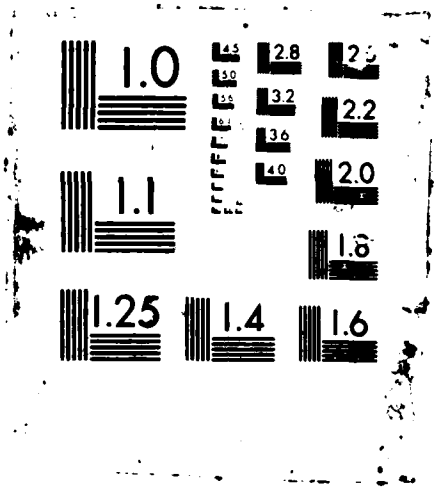
1.0
1.1
1.25
1.4
1.6
2.8
3.2
3.6
4.0
2.2
2.0
1.8

CRREL
REPORT 86-16

US Army Corps
of Engineers
Cold Regions Research &
Engineering Laboratory

12

Triaxial testing of first-year sea ice

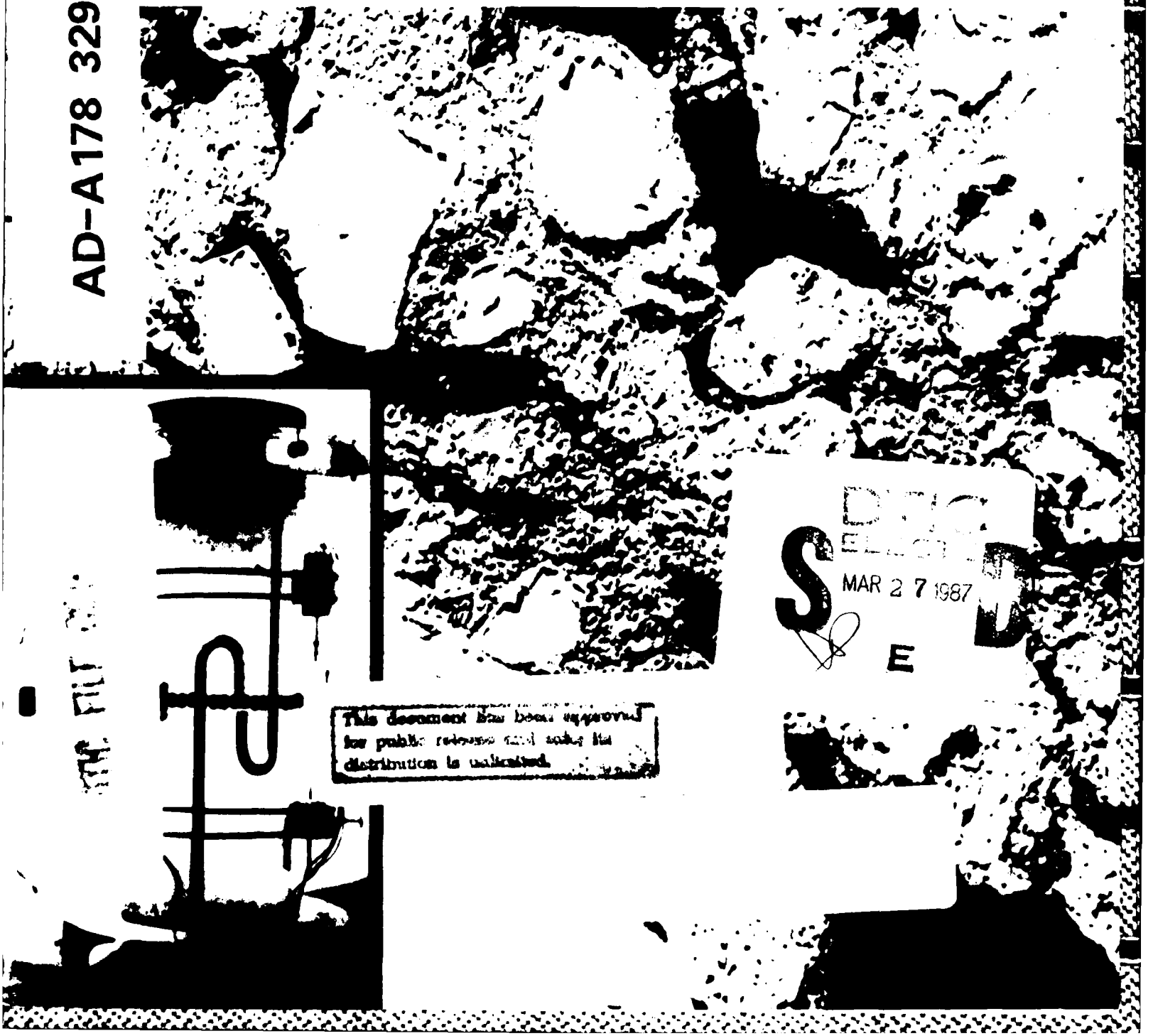

For conversion of SI metric units to U.S./British customary units of measurement consult ASTM Standard E380, Metric Practice Guide, *published by the American Society for Testing and Materials, 1916 Race St., Philadelphia, Pa. 19103.*

Cover: An instrumented test specimen superimposed over aerial photograph of pack ice in the Beaufort Sea.

UNCLASSIFIED
SECURITY CLASSIFICATION OF THIS PAGE

AD-A178 329

REPORT DOCUMENTATION PAGE

Form Approved
OMB No 0704-0188
Exp Date Jun 30, 1986

1a. REPORT SECURITY CLASSIFICATION UNCLASSIFIED	1b. RESTRICTIVE MARKINGS
2a. SECURITY CLASSIFICATION AUTHORITY	3. DISTRIBUTION/AVAILABILITY OF REPORT Approved for public release; distribution is unlimited.
2b. DECLASSIFICATION/DOWNGRADING SCHEDULE	
4. PERFORMING ORGANIZATION REPORT NUMBER(S) CRREL Report 86-16	5. MONITORING ORGANIZATION REPORT NUMBER(S)
6a. NAME OF PERFORMING ORGANIZATION U.S. Army Cold Regions Research and Engineering Laboratory 6b. OFFICE SYMBOL (If applicable) CRREL	7a. NAME OF MONITORING ORGANIZATION Sohio Petroleum Company
6c. ADDRESS (City, State, and ZIP Code) Hanover, New Hampshire 03755-1290	7b. ADDRESS (City, State, and ZIP Code)
8a. NAME OF FUNDING/SPONSORING ORGANIZATION 8b. OFFICE SYMBOL (If applicable)	9. PROCUREMENT INSTRUMENT IDENTIFICATION NUMBER
8c. ADDRESS (City, State, and ZIP Code)	10. SOURCE OF FUNDING NUMBERS PROGRAM ELEMENT NO. / PROJECT NO / TASK NO / WORK UNIT ACCESSION NO

11. TITLE (Include Security Classification)

TRIAXIAL TESTING OF FIRST-YEAR SEA ICE (Unclassified)

12. PERSONAL AUTHOR(S)

J.A. Richter-Menge, G.F.N. Cox, N. Perron, G. Durell and H.W. Bosworth

13a. TYPE OF REPORT	13b. TIME COVERED	14. DATE OF REPORT (Year, Month, Day)	15. PAGE COUNT
	FROM _____ TO _____	December 1986	47

16. SUPPLEMENTARY NOTATION

17. COSATI CODES			18. SUBJECT TERMS (Continue on reverse if necessary and identify by block number)
FIELD	GROUP	SUB-GROUP	First-year sea ice; Mechanical properties; Ice; Sea ice; Ice properties

19. ABSTRACT (Continue on reverse if necessary and identify by block number)

This report presents the first series of conventional triaxial tests carried out on columnar first-year sea ice samples obtained from the field and tested under controlled laboratory conditions using a large-capacity test machine. A total of 110 horizontal ice samples from Prudhoe Bay, Alaska, were tested on a closed-loop electro-hydraulic test machine at -10°C in unconfined and confined constant-strain-rate compression. The confined tests were conducted in a conventional triaxial cell ($\sigma_1 > \sigma_2 = \sigma_3$) that maintained a constant ratio between the radial and axial stress (σ_2/σ_1 = constant) to simulate in situ loading conditions. The load ratios used were 0.25, 0.50 and 0.75. The strain rate of each test was constant at 10^{-2}, 10^{-3}, or 10^{-5} s^{-1}. Data are presented on the strength, failure strain and initial tangent modulus of the first-year sea ice under these loading conditions. The effects of confining pressure, strain rate and ice structure on the mechanical properties of the ice are examined.

20. DISTRIBUTION/AVAILABILITY OF ABSTRACT	21. ABSTRACT SECURITY CLASSIFICATION
☒ UNCLASSIFIED/UNLIMITED ☐ SAME AS RPT ☐ DTIC USERS	UNCLASSIFIED
22a. NAME OF RESPONSIBLE INDIVIDUAL J.A. Richter-Menge	22b. TELEPHONE (Include Area Code) 603-646-4266 / 22c. OFFICE SYMBOL CRREL-RS

DD FORM 1473, 84 MAR — 83 APR edition may be used until exhausted. All other editions are obsolete.

SECURITY CLASSIFICATION OF THIS PAGE
UNCLASSIFIED

A

PREFACE

This report was prepared by Jacqueline A. Richter-Menge, Research Civil Engineer, Dr. Gordon F.N. Cox, Research Geophysicist, Nancy Perron, Physical Science Technician, and Hazen Bosworth, Physical Science Technician, all of the Snow and Ice Branch, Research Division; and Glenn Durell, Mechanical Engineering Technician, of the Technical Services Division, U.S. Army Cold Regions Research and Engineering Laboratory. This study was sponsored by the Sohio Petroleum Company with support from Amoco Production Company, Exxon Production Research Company, Marathon Oil Company and Mobil Research and Development Company.

The authors thank T. Walden of Sohio Petroleum Company and T. Ralston of Exxon Production Research Company for technically reviewing the manuscript of this report. In addition the authors express their appreciation to T. Tucker and T. Misiak for their support and cooperation during the field program.

CRREL Report 86-16

December 1986

Triaxial testing of first-year sea ice

J.A. Richter-Menge, G.F.N. Cox, N. Perron, G. Durell and H.W. Bosworth

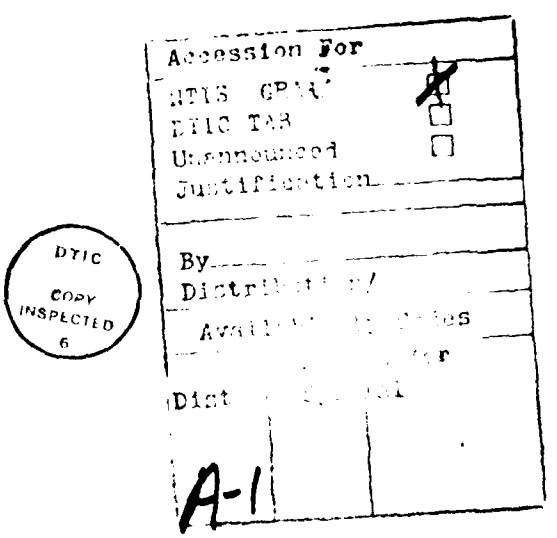

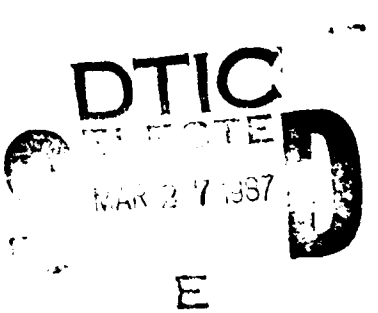

CONTENTS

	Page
Abstract	i
Preface	ii
Introduction	1
Field sampling	1
Site selection and description	1
Coring techniques	3
Shipping and storage of ice samples	5
Ice description	7
Structure	7
Salinity, density and temperature	8
Sample preparation and test techniques	9
Test variables and sampling scheme	15
Sample analysis	15
Structure	15
Salinity, density and porosity	16
Test results	17
Strength	17
Failure strains	27
Initial tangent modulus	30
Conclusions	31
Literature cited	32
Appendix A: Test results from the unconfined and confined constant-strain-rate compression tests	35

ILLUSTRATIONS

Figure

1. Map of Prudhoe Bay showing location of sampling site	2
2. Sampling site	2
3. Barrel used to obtain 30.5-cm-diameter core	3
4. Modified post hole digger used to drill 30.5-cm-diameter vertical ice core	4
5. Marking magnetic north–south line on top of 30.5-cm-diameter ice core before drilling	4
6. Ice tongs used to retrieve 30.5-cm-diameter ice core	5
7. Taking field notes on a 160-cm-long, 30.5-cm-diameter, vertical ice core	6
8. Drill press used to obtain 10.8-cm-diameter horizontal samples from 30.5-cm-diameter vertical ice cores	6
9. Location of horizontally cored ice samples relative to the first-year columnar ice sheet	7
10. Vertical and horizontal thin sections showing the crystal structure of an ice core taken from the sampling area	8
11. Temperature, salinity and schematic structural profile of a vertical ice core taken from the sampling area	9
12. Closed-loop electrohydraulic testing machine	10
13. Testing machine control console and recording system	11

Figure Page
14. Instrumented unconfined compression test specimen 11
15. Schematic diagram of modified conventional triaxial cell 12
16. Conventional triaxial cell before modifications 13
17. Modified conventional triaxial cell 14
18. Instrumented confined compression test specimen 14
19. Sections used in the crystal structure analysis of the tested ice samples 16
20. Mean compressive strength of first-year sea ice samples vs strain rate 20
21. Compressive strength of first-year sea ice samples vs angle between applied load and crystal c-axes 21
22. Deformation of a tested specimen both perpendicular and parallel to the direction of crystal elongation 25
23. Mean deviatoric strength of first-year sea ice samples vs confining pressure at failure 26
24. Characteristic stress–strain curves of horizontal samples of first-year sea ice ... 27
25. Compressive strength of first-year sea ice samples vs strain at failure 28

TABLES

Table
1. Number of constant-strain-rate compression tests at different confinement ratios, strain rates and estimated σ:c angles 15
2. Mean σ:c angle of horizontal samples of columnar first-year sea ice measured in the laboratory using Rigsby Universal Stage 16
3. Mean salinity, density and porosity of first-year sea ice samples 18
4. Mean compressive strength of horizontal samples of columnar first-year sea ice 19
5. Ratio of mean compressive strength between estimated σ:c angle groups of horizontal samples of columnar first-year sea ice 24
6. Characteristic stress–strain curves of horizontal samples of first-year sea ice ... 27
7. Mean axial strain at failure for horizontal samples of columnar first-year sea ice 30
8. Mean initial tangent modulus of horizontal samples of columnar first-year sea ice 31

Triaxial Testing of First-Year Sea Ice

J.A. RICHTER-MENGE, G.F.N. COX, N. PERRON,
G. DURELL AND H.W. BOSWORTH

INTRODUCTION

The behavior of columnar first-year sea ice tested under uniaxial compression has been the topic of many investigations. These studies have shown that the mechanical properties of the columnar ice are anisotropic because of the inherent structural characteristics of the material. Recently, more work has been done to define the behavior of columnar ice when it is subjected to more complex stress states. Tests by Hausler (1981) on unaligned, columnar saline ice, grown in the laboratory, using true multi-axial loading states ($\sigma_1 \neq \sigma_2 \neq \sigma_3$) are the most notable. Nawwar et al. (1983) have also tested laboratory-grown saline ice under conventional triaxial test conditions ($\sigma_1 \neq \sigma_2 = \sigma_3$). Directionally confined compression tests ($\sigma_1 \neq \sigma_2$, $\sigma_3 = 0$) using columnar first-year sea ice have been done in the field by Timco and Frederking (1983). Sinha (1985) has also done directionally confined tests on second-year columnar ice samples. Results from all of these confined tests are more indicative of in situ loading conditions and are required to develop yield criterion for the design of offshore structures and vessels for the Arctic.

This report augments the existing data base by presenting the first series of conventional triaxial tests performed on columnar first-year sea ice samples obtained from the field and tested under controlled laboratory conditions using a large-capacity test machine. A total of 110 horizontal ice samples from Prudhoe Bay, Alaska, were tested in unconfined and confined constant-strain-rate compression. The confined tests were conducted in a conventional triaxial cell that maintained a constant ratio between the radial and axial stress (σ_2/σ_1 = constant). Three strain rates and one temperature were investigated. All of the columnar ice samples exhibited alignment of the crystallographic c-axes in the horizontal plane, which allowed us to study the influence of confinement on the anisotropic behavior of the ice in the plane of the ice sheet.

FIELD SAMPLING

The field sampling for this program was conducted during April 1983 in conjunction with the British Petroleum (BP) *Mobile Ice Testing Laboratory Field Program*. On 2 April, we selected a site based on the presence of aligned, columnar first-year sea ice that was required for both our study and the BP study. An area of 100 m² was marked off for sampling. From this area we obtained a total of 27.4 m of 30.5-cm (12-in.) diameter vertical ice core for our study. This ice provided us with 105 potential 10.8-cm (4¼-in.) diameter horizontal test samples. An additional 18 horizontal samples were obtained from vertical ice cores provided by Sohio. This ice had also been taken from the 100-m² sampling area during the 1983 field program but was stored in Cleveland, Ohio, until mid-January 1984.

Site selection and description

The sampling site was located in the Alaskan Beaufort Sea approximately 9 miles from Prudhoe Bay (Fig. 1). This site was chosen for several reasons. First, it was situated between the Alaskan mainland and the barrier islands. In this area the fast ice growth is generally undisturbed and is influenced by a predominately east-west longshore current. According to Weeks and Gow (1978), these conditions promote the growth of strongly aligned, columnar sea ice. Also, 9 miles from the coast the water depths were great enough to permit the ice sheet to grow to its full depth, well above the ocean floor.

At the 9-mile site, the surface of the ice was smooth, indicating little disturbance during initial growth (Fig. 2). Beyond the site and extending

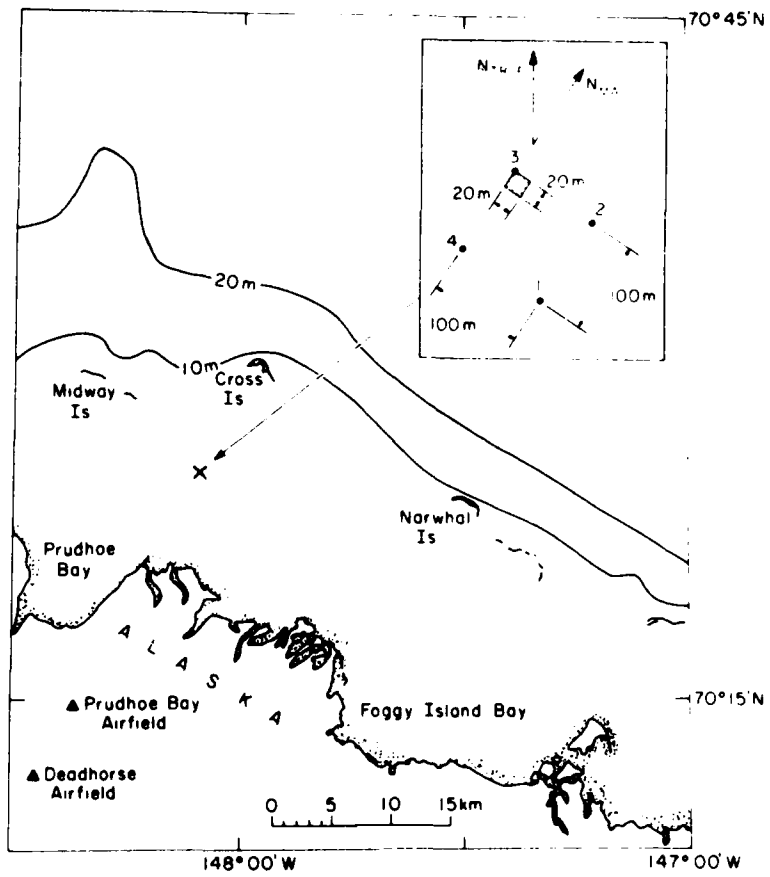

Figure 1. Map of Prudhoe Bay showing location of sampling site. Shaded portion of inset represents area from which all samples were cored.

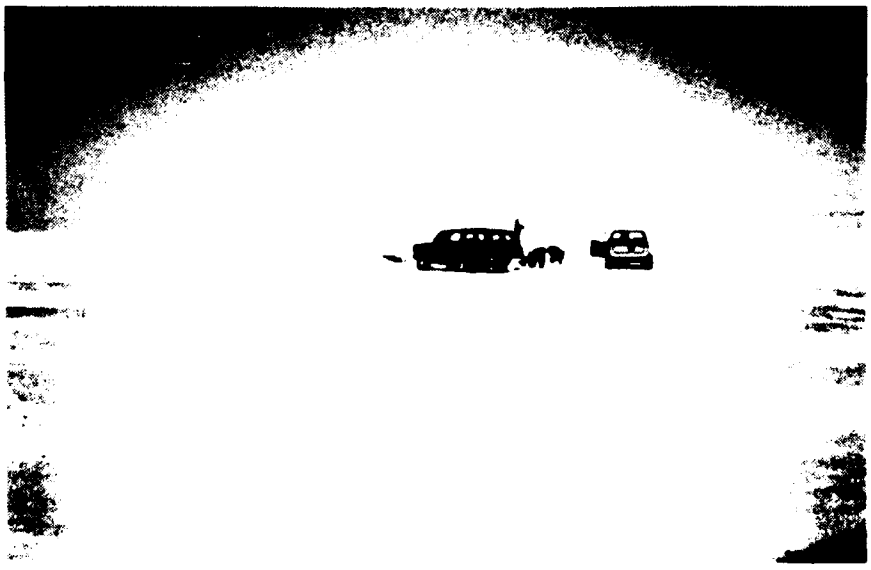

Figure 2. Sampling site. Rubble in foreground was created by snowplow.

north to Cross Island, the ice surface was rough, consisting of broken blocks of ice approximately 20 cm thick. A sampling area of 100 m² was marked off using flags at the corner points (inset, Fig. 1). Flags 1 and 2, and 3 and 4 were aligned with the magnetic N–S direction to give us a visual reference during sampling. At each flag a continuous 10.8-cm-diameter vertical ice core was taken to determine the lateral continuity of the ice structure and the c-axes orientation within our chosen sampling area. All of the horizontal ice samples used in this study were located in a 20-m² area near flag 3.

Coring techniques

The continuous vertical cores taken at each of the flagged corners were obtained using the CRREL 4¼-in.-diameter (10.8-cm-diam.) Fiberglas coring auger (Rand and Mellor 1985). All of the horizontal samples collected for testing were taken from 30.5-cm-diameter vertical ice cores. A 30.5-cm-diameter Fiberglas coring auger was mounted on a specially modified gasoline-powered post hole digger as shown in Figure 3. This coring auger was designed to obtain vertical ice samples up to 1 m in length. The modified post hole digger, pictured in Figure 4, provided the necessary rotational power for drilling the 30.5-cm-diameter ice core and was equipped with a winch system capable of removing core from the drill hole.

The following procedure was used to obtain the large diameter core and the 10.8-cm-diameter horizontal ice samples. The 30.5-cm core barrel was lowered to the surface of the ice and turned by hand to scribe an outline of the core. The core barrel was then lifted and a line corresponding to magnetic N–S was etched across the top of the core (Fig. 5). Magnetic north was indicated using a crossmark. The 30.5-cm core barrel was again lowered and drilling began. Approximately 80 cm of ice was augered and the core barrel was re-

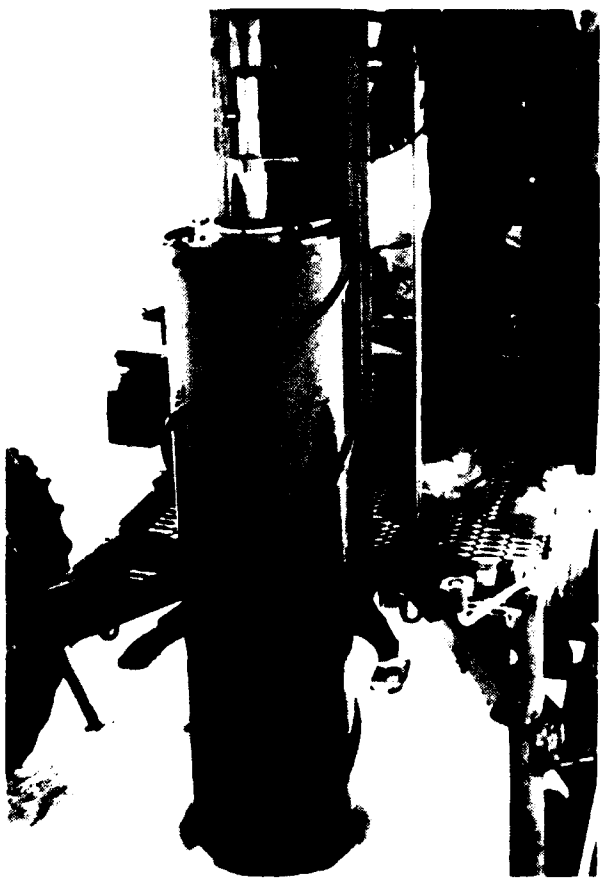

Figure 3. Barrel used to obtain 30.5-cm-diameter core.

Figure 4. Modified post hole digger used to drill 30.5-cm-diameter vertical ice core.

Figure 5. Marking magnetic north-south line on top of 30.5-cm-diameter ice core before drilling.

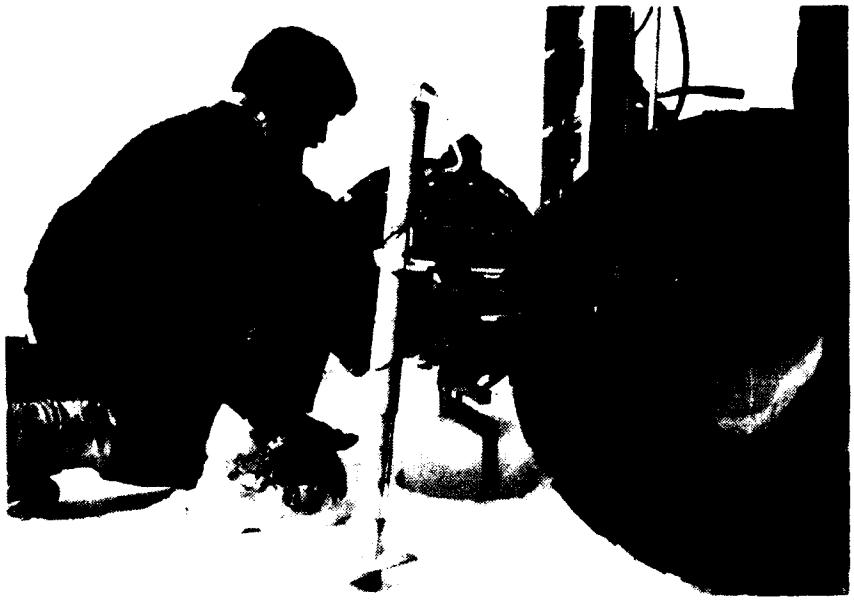

Figure 6. Ice tongs used to retrieve 30.5-cm-diameter ice core.

moved from the hole. The ice core was then sheared at the bottom of the drill hole and a simple core retrieval system was used to recover the 30.5-cm-diameter length of ice (Fig. 6). The core retrieval system consisted of specially designed ice tongs that were hooked to the cable of the winch system with a clamp. The tension in the cable provided the force necessary for the ice tongs to grab and hold the large core as it was removed from the drill hole. Once the core was on the surface of the ice it was placed on its side. A line was scored along the length of the core to indicate magnetic north. Field notes were made describing the total length of the core, the temperature of the ice at specific locations, and any unusual structural characteristics (Fig. 7). An additional 80-cm length of 30.5-cm-diameter core was obtained down hole using an aluminum extension rod. The location of magnetic north was also indicated on this core.

The platelet structure at the bottom of the deepest core was observed to estimate the c-axes direction relative to the magnetic north line. At this location in the core the characteristic platelet structure of the aligned, first-year columnar sea ice was generally well-defined. The crystallographic c-axes are perpendicular to the direction of the platelets. The 30.5-cm-diameter core was then placed on its side, in a drill press with a 10.8-cm-diameter hole saw (Fig. 8). The core was rotated to obtain horizontal samples with an orientation of 0°, 90° or 45° (Fig. 9) to the c-axes direction, as estimated by observing the platelet structure. The cylindrical horizontal samples were taken along the length of the 30.5-cm-diameter core. Their exact depth and the estimate of the angle between the cylindrical axis of the sample and the c-axes were noted in the field book.

Shipping and storage of ice samples

After a horizontal ice sample was obtained and cataloged, it was packed in a numbered, 1-m-long core tube. Notes were taken to document the core tube number and the sample location within the core tube. Gaps in the core tubes were packed with paper to protect the core ends from damage during shipping. The core tubes were then placed in insulated shipping boxes that were constructed of heavy-weight, wax-coated cardboard with 7.5-cm-thick styrofoam insulation on the bottom, sides and top. Each box could accommodate six 1-m-long tubes, snow for packing and dry ice for refrigeration during shipping. The shipping boxes containing the ice were stored outside until ambient temperatures required us to move them into a refrigerated facility in Deadhorse. No problems were experienced with brine drainage.

The ice samples were shipped directly to Boston from Deadhorse via air cargo. Before shipping, each box was packed with 5 to 7 cm of snow and

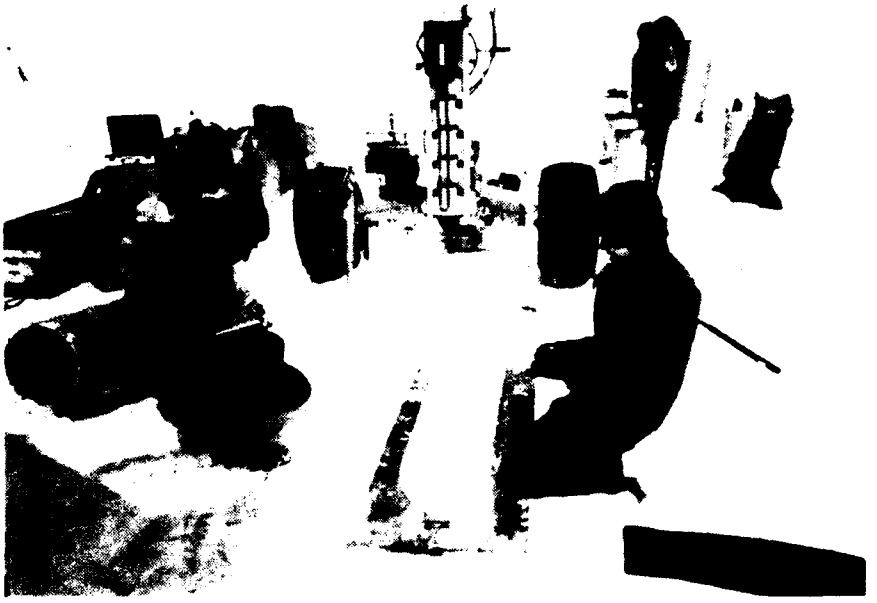

Figure 7. Taking field notes on a 160-cm-long, 30.5-cm-diameter, vertical ice core.

Figure 8. Drill press used to obtain 10.8-cm-diameter horizontal samples from 30.5-cm-diameter vertical ice cores.

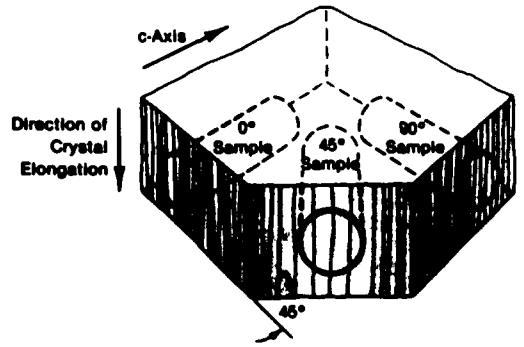

Figure 9. Location of horizontally cored ice samples relative to the first-year columnar ice sheet.

charged with 34 kg of dry ice. The snow was placed on top of the core tubes to prevent thermal cracking of the ice cores, which might result from direct contact with the dry ice. CRREL personnel transferred the ice from Boston to Hanover in a refrigerated truck. The core tubes containing the ice were then immediately removed from the shipping boxes and stored in a coldroom at -30°C. The ice remained at this temperature until a sample was selected for use in a mechanical properties test.

ICE DESCRIPTION

The ice in the 100-m² sampling area was laterally uniform with respect to structure, salinity and temperature at a given depth. The total depth of the ice sheet varied from 2.0 to 2.05 m.

Structure

Several 10.8-cm-diameter vertical ice cores were taken in the sampling area specifically for salinity and petrographic analysis. In Figure 10, horizontal and vertical ice thin sections from one of these cores are shown photographed between crossed polarizers. As discussed in Tucker et al. (1984), the upper 5 cm of the core is composed of randomly oriented granular ice with an average grain size of 1.5 mm. The structure changes from granular to columnar ice from 5 to 10 cm. Below 10 cm the ice is columnar with the c-axes lying in the horizontal plane of the ice sheet. This growth sequence is typical of sea ice formed in quiet water conditions and has been discussed previously by Gow and Weeks (1977). The columnar ice growth is interrupted by a band of extremely fine grained (0.5 mm) granular ice from 20 to 29 cm. At 29 cm the structure again becomes columnar with c-axes horizontal. The columnar ice structure continues to the bottom of the core without further interruption. The grain size and degree of alignment of the c-axes in the columnar ice increase with depth in accordance with observations made by Weeks and Gow (1978, 1980). The alignment of the c-axes in the horizontal plane is approximately east-west, which is also in close agreement with alignment measurements made by Weeks and Gow (1978) in sea ice samples from the same area.

The granular ice band from 20 to 29 cm contained a very fine clayey sediment. This sediment band was widespread throughout the sampling area and often occurred below a layer of congelation or columnar ice. This implied that quiet water growth conditions had existed before the formation of the sediment-laden layer. Reviewing meteorological data from the Prudhoe Bay vicinity between October and November 1982, we speculate that there was a storm or storms with high southwesterly winds during the latter part of October. This storm caused the young sheet of fast ice to break up into loosely packed floes approximately 20 cm thick. Frazil ice then formed in the open leads, as described by Martin (1981). The turbulent water also caused fine clay sediments from the ocean floor to become incorporated into the water column in shallow depth areas. The suspended sediment mixed with the frazil ice and as wave action continued, some of the sediment-laden frazil was advected under the adjacent ice floes. This ice then froze in place. Later, the ice sheet consolidated again and congelation ice began to form under the sediment-laden ice layer. This mechanism for the incorporation of sediment into ice has been observed previously and is discussed in Larsen (1980). Cores taken from various locations in the sample area showed sediment bands at depths varying from 2 to 40 cm. The thickness of the sediment band also varied from core to core. Therefore, to assure us of columnar test specimens, all horizontal samples were taken at depths greater than or equal to 60 cm.

Figure 10. Vertical and horizontal thin sections showing the crystal structure of an ice core taken from the sampling area (Tucker et al. 1984).

Salinity, density and temperature

The salinity and temperature profiles of the core just discussed are shown in Figure 11, along side of a schematic structure profile. The variation of salinity with depth is in good agreement with observations made by Nakawo and Sinha (1981) on first year ice sheets. The salinity profile has previously been characterized as C-shaped, with a high salinity at the top and bottom of the ice sheet. The center portion of the ice sheet has a lower salinity, which is nearly constant. In our case the salinity in the center of the sheet varied from 3.5 to 4.5‰. An area of high salinity corresponding to the location of the sediment-laden ice was observed in all of the cores sampled.

The temperature profile of the ice sheet was nearly linear, increasing with depth from the ambient temperature at the top of the ice sheet to the freezing point of sea water (-1.8°C) at the bottom of the ice sheet. This temperature distribution is typical of late winter conditions.

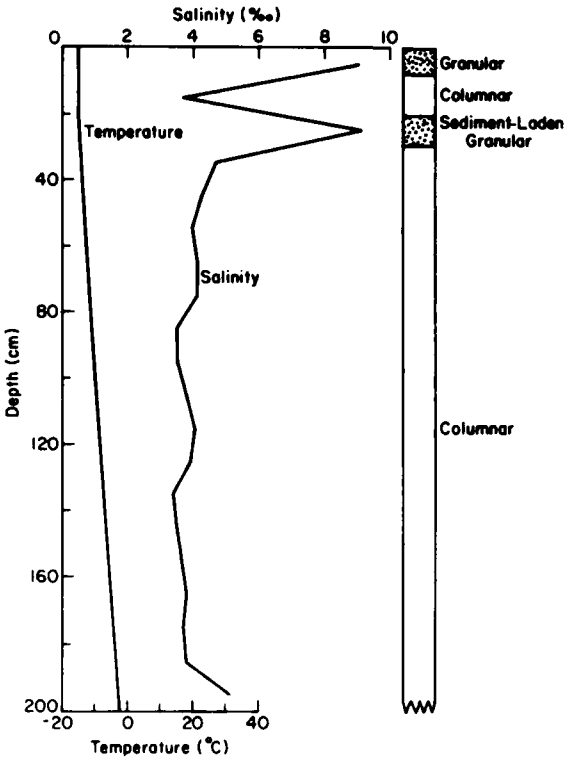

Figure 11. Temperature, salinity and schematic structural profile of a vertical ice core taken from the sampling area.

SAMPLE PREPARATION AND TEST TECHNIQUES

The sample preparation techniques and testing method for the unconfined compression tests were originally developed for a study involving samples of multi-year sea ice ridges. These methods and techniques are briefly described below. For a more detailed report on the subject the reader is referred to Mellor et al. (1984).

Dumbbell-shaped specimens were prepared from the 10.8-cm-diameter horizontal ice cores. Samples were first rough-cut on a bandsaw, and the ends were milled square on a milling machine to produce a 25-cm-long test specimen. Synthane end caps were then bonded to the sample using fresh water to freeze them to the milled end planes. The samples with end caps were turned on a lathe to a dumbbell shape, with a neck diameter of 10.16 cm. The form tool used to prepare the dumbbell compression specimens had a radius of curvature of 20.32 cm, twice the diameter of the finished neck. This radius was chosen to minimize stress concentrations near the sample end planes. Every effort was made to produce properly sized, precision-machined test samples using recommended methods (Hawkes and Mellor 1972, Schwarz et al. 1981).

Once the ice sample was given end caps and machined, a comparator was used to see if the sample ends were parallel and square. The comparator was run along the outside perimeter of the top end cap and the difference or maximum variation in sample height was noted at the low point. Before the unconfined or confined compression test was performed, an amount of steel shimstock, equivalent to the variation noted on the top end cap, was placed at the low point. The loading device was then brought into contact with the top end cap. The results of the tests in this program and in other test programs using the same preparation techniques (Mellor et al. 1984) indicate that shimming is an effective way for correcting for the lack of parallelism in compression tests using samples with end caps.

The average sample height variation in this series of tests was 0.036 $\pm$0.028 cm. This variation was significantly higher than the average 0.010-cm

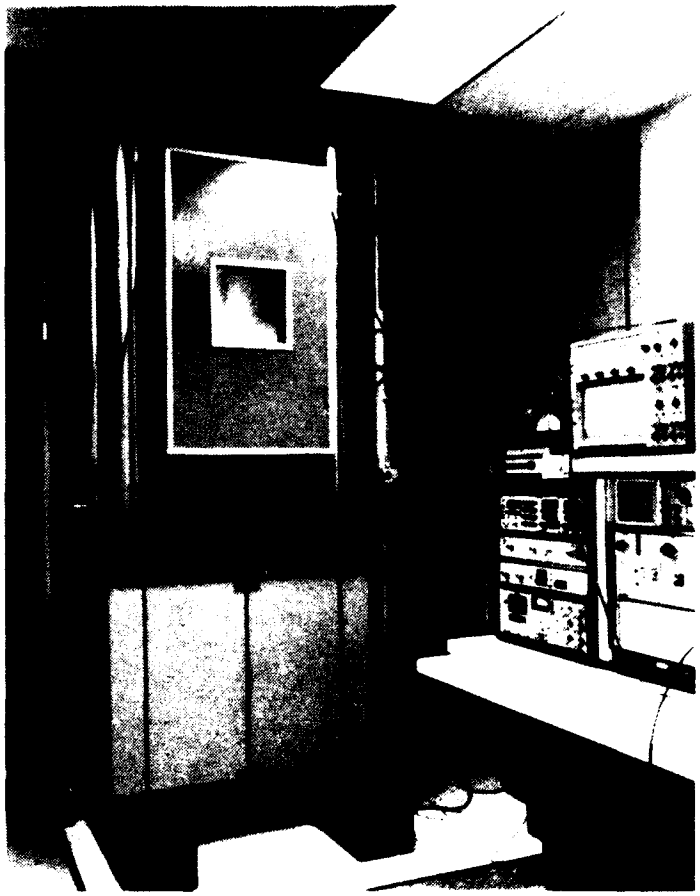

Figure 12. Closed-loop electrohydraulic testing machine (loading frame and environmental cabinet).

variation observed using the same endcapping equipment in our other test programs. This difference was the result of the initial core quality. In our previous tests we had primarily used vertically cored ice that was of extremely good quality with respect to its cylindrical shape. The horizontal coring jig wobbled, however, and produced cores with a large bulge in the center. Consequently, our endcapping jig was not able to correct for the lack of parallelism present after milling. We have now developed an endcapping method at CRREL that does not depend on core quality (Cole et al. 1986).

All of the compression tests, confined and unconfined, were conducted on the closed-loop electrohydraulic testing machine pictured in Figure 12. The machine had two actuators with capacities of 1.1 and 0.11 MN and a fast-response, high-flow-rate servo-valve. The load frame of the machine had a capacity of 2.2 MN. Test temperatures were controlled within 0.5°C by placing the sample in an environmental chamber mounted between the columns of the testing machine. The lower machine platen was also refrigerated to eliminate any thermal gradient problems. Load and sample strain data were recorded on an XY plotter, a strip chart and an FM magnetic tape recorder (Fig. 13).

Strain rates in the unconfined uniaxial compression tests were controlled by monitoring the full sample strain with an extensometer, which was attached to the synthane end caps that were bonded to the test specimen (Fig. 14). Strains on the necks of the specimens were also monitored with a pair of Direct Current Displacement Transducers (DCDTs) to provide accurate strain, strain-rate and modulus data. The unconfined tests were programmed to continue to 5% full sample strain to examine post-yield behavior and the residual strength of the ice. Since this resulted in considerable deformation of the test specimen, strain rates could not be controlled by the transducers mounted on the ice.

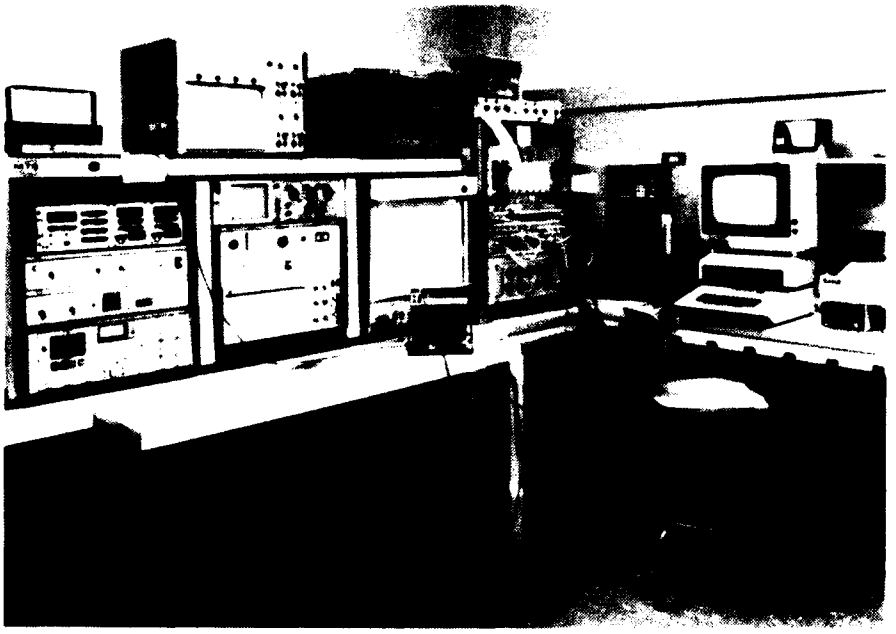

Figure 13. Testing machine control console and recording system.

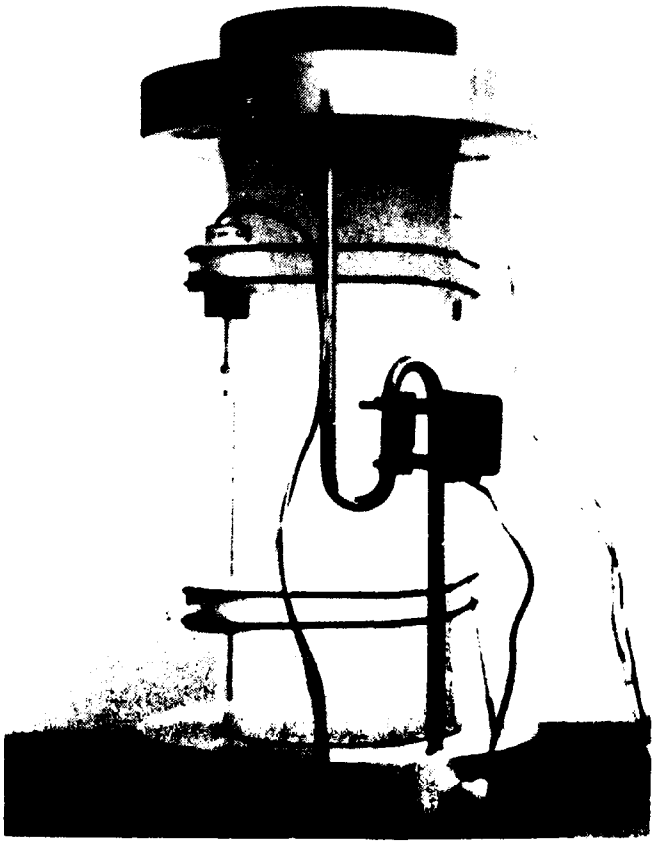

Figure 14. Instrumented unconfined compression test specimen.

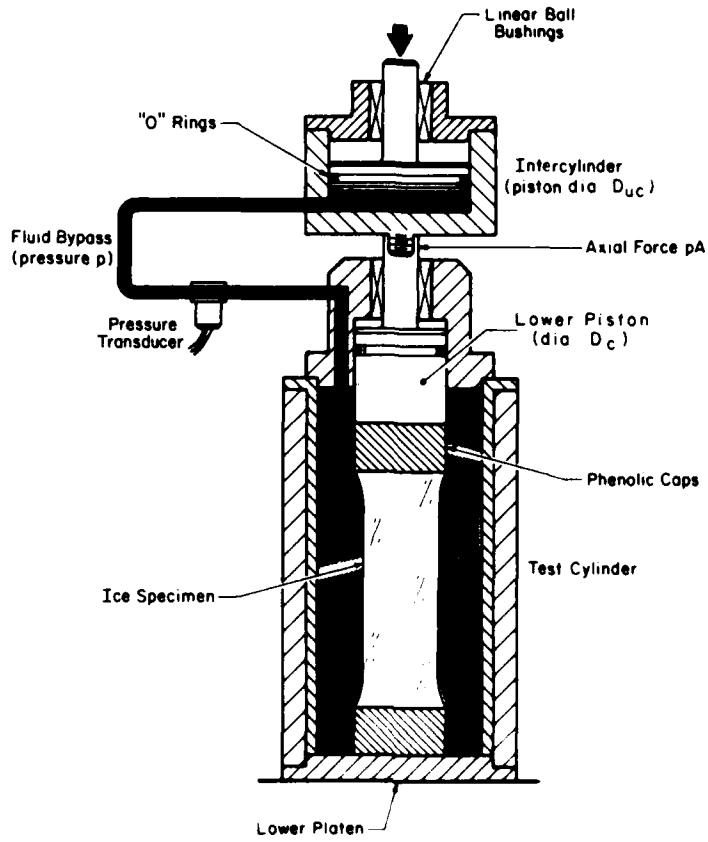

Figure 15. Schematic diagram of modified conventional triaxial cell.

Confined compression tests were done using the triaxial cell shown schematically in Figure 15. The cell was designed so that the radial confining pressure increased in constant proportion to the applied axial stress. Three ratios of radial stress to axial stress were used: 0.25, 0.50 and 0.75. For a right circular cylindrical specimen, the ratio of the confining pressure to the axial stress is defined by the ratio of the diameter of the piston entering the cell (D_c = 10.67 cm) to the diameter of the piston in the upper cylinder (D_{uc}). A correction must be made in determining D_{uc}, however, to account for the dumbbell shape of our specimens. The confining fluid reacts against the filletted ends of the sample, reducing the overall axial compressive stress being applied to the sample. As a result of this reaction, D_{uc} must be increased to proportionally reduce the radial stress. The larger ratios were obtained by placing the appropriate reduction collar in the upper piston and using a correspondingly smaller diameter piston. Hydraulic fluid was used as the confining medium. A latex membrane was placed around the test specimen to prevent the permeation of hydraulic fluid into the sample void spaces.

In early confined compression tests (indicated in Appendix A), the strain rate was controlled by the averaged output of two extensometers mounted on the shaft going into the triaxial cell (Fig. 16). Since we assumed that the extensometers mounted on the shaft would give reliable sample strain measurements, no instrumentation was placed directly on the sample for the measurement of strain. During the analysis of the data from these early tests, however, we found that the confined initial tangent modulus values were consistently lower than the initial tangent moduli measured in the unconfined tests. This caused some concern because we intuitively expected the confined modulus to be greater. Any confinement should reduce the axial displacement for a given load, thereby increasing the measured modulus.

After a series of tests described in Cox and Richter-Menge (1985) and Richter-Menge (1984),

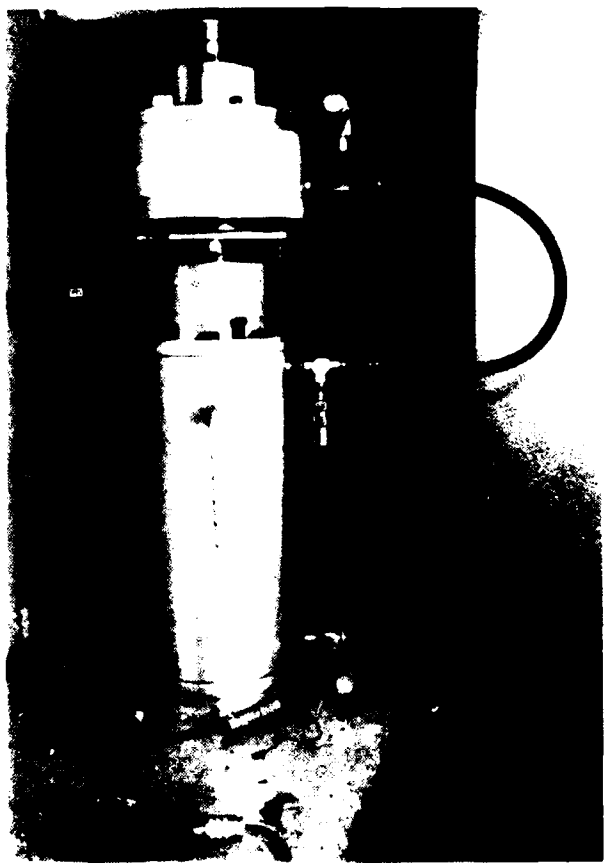

Figure 16. Conventional triaxial cell before modifications.

it became clear that closure between the lower piston and the top end cap was significant at the beginning of the test when the ice displacements were small. Since we were using extensometers mounted on the shaft of the triaxial cell to measure ice displacement, this closure was included in the measurement. This gave us higher displacement measurements than were actually occurring in the ice. This, in turn, resulted in the reduction of the initial tangent modulus by as much as one half the value that would have been obtained in an unconfined test on the same sample. (In the unconfined tests, sample displacement measurements were made directly on the ice and did not include any loading train displacements). As the axial force continued to increase in the confined test, the ice displacement continued to increase while the displacement across the interface remained constant. This meant that the closure had a significant influence on the axial displacement measurements only during the initial portion of the test.

To obtain reliable initial tangent moduli and accurate sample strains throughout the confined compression tests, it was necessary to modify the triaxial cell so that it could accommodate an instrumented sample. The cell was enlarged (Fig. 17) and the sample was instrumented with a pair of Linear Variable Differential Transducers (LVDTs). The LVDTs chosen for these tests are immersible and are capable of withstanding high hydraulic pressures and low temperatures. The LVDTs were used to measure sample displacement and to control the ice strain rate. Since we were still interested in examining the post-yield behavior of the ice, the LVDTs were mounted on the sample end caps (Fig. 18). The LVDTs had a maximum travel of 0.64 cm, which translated to a maximum sample displacement of 2.5% at the end of the test. This method of measuring sample strains in the confined compression tests proved to be extremely successful and was used throughout the remainder of the test program.

Figure 17. Modified conventional triaxial cell.

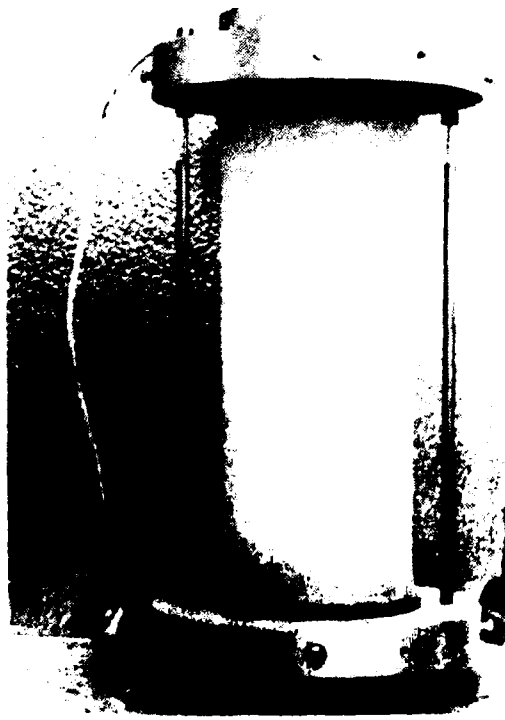

Figure 18. Instrumented confined compression test specimen.

Corrections have been made for the sample strain measurements and secant moduli for those confined compression tests performed with the extensometers mounted on the shaft of the triaxial cell using the equations developed in Cox and Richter-Menge (1985). It has been shown that these corrections are extremely accurate for all strain measurements, with the exception of the initial tangent modulus. For this reason the initial tangent moduli for the early tests are not included in Appendix A.

TEST VARIABLES AND SAMPLING SCHEME

A total of 110 constant-strain-rate compression tests were performed on the horizontal, columnar first-year sea ice samples. Of the tests, 30 were run in uniaxial compression with no confinement. The remaining 80 tests were done in a conventional triaxial cell ($\sigma_1 > \sigma_2 = \sigma_3$), designed to provide a constant ratio between the radial or confining pressure ($\sigma_r = \sigma_2 = \sigma_3$) and the axial stress ($\sigma_a = \sigma_1$). The load ratios ($\sigma_r/\sigma_a$) used in the confined compression tests were 0.25, 0.50 and 0.75. These confining ratios were chosen to provide an adequate range of data for the development of yield surfaces.

All of the tests were executed at one temperature: -10°C. The strain rate of each test was constant at 10^{-2}, 10^{-3} or 10^{-5} s^{-1}. The estimated angle between the load and mean c-axes direction (σ:c) was 0°, 90° or 45°. We did a minimum of four tests at each test condition; the number of tests at each condition is given in Table 1. When possible, we tried to provide four horizontal samples at one test condition that had been obtained from the same 30.5-cm-diameter ice core. As a result of our field sampling procedures described earlier, these samples tended to have the same mean σ:c angle. The degree of alignment of the c-axes in the horizontal plane, however, tended to increase with an increase in depth. Consequently, using samples from the same 30.5-cm core provided us with an opportunity to observe the effect of the degree of c-axes alignment on sample strength.

Originally, we had planned to do four 10^{-2} s^{-1} tests at each confinement ratio using samples with an estimated σ:c angle of 45°. We successfully ran a series of 10^{-2} s^{-1} tests for the unconfined loading case, but we were unable to complete a satisfactory test at any of the remaining confinement ratios. Two limitations prevented us from performing these tests. First, at a strain rate of 10^{-2} s^{-1} and confining ratio of 0.75 the capacity of the triaxial cell (2700 lb/in.^{2} [18.6 MPa]) was far exceeded. Second, the viscosity of the hydraulic fluid at -10°C was too high to maintain a constant σ_r/σ_a ratio at strain rates of 10^{-2} s^{-1}. In other words, the confining fluid was traveling too slowly between the test chamber and the upper piston housing (see Fig. 12) relative to the speed of the piston entering the triaxial cell. Both of these problems could have been solved with further modifications to the triaxial cell, but project costs and time prohibited this.

Table 1. Number of constant-strain-rate compression tests at different confinement ratios (σ_r/σ_a), strain rates and estimated σ:c angles (test temperature = -10°C).

	σ:c		
	0°	90°	45°
	σ_r/σ_a = 0.0*		
$\dot{\epsilon}$ = 10^{-2} s^{-1}	—	—	4
$\dot{\epsilon}$ = 10^{-3} s^{-1}	4	4	6
$\dot{\epsilon}$ = 10^{-5} s^{-1}	4	4	4
	σ_r/σ_a = 0.25		
$\dot{\epsilon}$ = 10^{-3} s^{-1}	6	4	4
$\dot{\epsilon}$ = 10^{-5} s^{-1}	7	4	4
	σ_r/σ_a = 0.50		
$\dot{\epsilon}$ = 10^{-3} s^{-1}	4	4	4
$\dot{\epsilon}$ = 10^{-5} s^{-1}	4	4	4
	σ_r/σ_a = 0.75		
$\dot{\epsilon}$ = 10^{-3} s^{-1}	6	5	4
$\dot{\epsilon}$ = 10^{-5} s^{-1}	4	4	4
Total	39	33	38

* Unconfined compression test.

SAMPLE ANALYSIS

Structure

The structural characteristics of the unconfined and confined test specimens were evaluated by preparing ice thin sections according to the techniques described in Weeks and Gow (1978). The test samples were sectioned after testing (Fig. 19). Two "vertical" thin sections (in the direction of

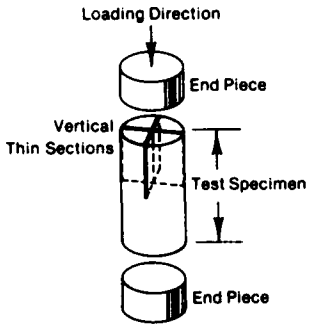

Figure 19. Sections used in the crystal structure analysis of the tested ice samples.

the load) were cut from the tested sample, one perpendicular to the other. One vertical thin section was made in the direction parallel to the plane of the original ice sheet. Since we were interested in measuring the angle between the load and the mean c-axes direction (σ:c), we took the vertical thin sections from the least disturbed portion of the tested sample. Early work indicated that there was some crystal rotation due to loading in the highly deformed areas. End pieces were taken from ice immediately adjacent to the sample to provide structural information should the sample be destroyed during the test. All thin sections were photographed between cross polarizers to provide a permanent structural record of each sample.

All of the test specimens were columnar and measurements of the crystallographic c-axes orientation in each sample were made using a Rigsby Universal Stage (Langway 1958). These measurements provided us with information on the mean angle between the c-axes and the load direction (σ:c). Recall that our previous σ:c designation of 0°, 90° or 45° was only an estimate made in the field. We also noted the standard deviation of the c-axes measurement from the mean σ:c angle to evaluate the effect of the degree of alignment of the c-axes in the horizontal plane on the compressive strength of the columnar ice samples. The measured mean σ:c angle for the samples, grouped according to test condition, are presented in Table 2. Comparison of the actual σ:c measurements to the estimated value of 0°, 90° or 45° shows that, in general, the field estimates were accurate to within 10° for the 0° and 90° samples. The variation in the estimate for the 45° samples averaged 15° with one notable exception. The samples from core D that were estimated to be 45° samples had a mean

Table 2. Mean σ:c angle (degrees) of horizontal samples of columnar first-year sea ice measured in the laboratory using Rigsby Universal Stage.

	σ:c*		
	0°	90°	45°
	σ_r/σ_a = **0.0**†		
$\dot{\epsilon} = 10^{-2}$ s^{-1}	—	—	36.8 ±8.2 (4)**
$\dot{\epsilon} = 10^{-3}$ s^{-1}	6.8 ±3.9 (4)	87.3 ±4.9 (4)	43.3 ±9.5 (6)
$\dot{\epsilon} = 10^{-5}$ s^{-1}	3.3 ±1.9 (4)	84.3 ±3.8 (4)	39.3 ±6.9 (4)
	σ_r/σ_a = **0.25**		
$\dot{\epsilon} = 10^{-3}$ s^{-1}	5.3 ±2.6 (6)	86.0 ±2.2 (4)	38.3 ±3.8 (4)
$\dot{\epsilon} = 10^{-5}$ s^{-1}	3.4 ±3.3 (7)	81.2 ±3.7 (4)	34.0 ±3.9 (4)
	σ_r/σ_a = **0.50**		
$\dot{\epsilon} = 10^{-3}$ s^{-1}	7.0 ±2.9 (4)	87.8 ±1.7 (4)	16.0 ±10.4 (4)
$\dot{\epsilon} = 10^{-5}$ s^{-1}	4.8 ±3.9 (4)	86.3 ±3.1 (4)	44.0 ±7.7 (4)
	σ_r/σ_a = **0.75**		
$\dot{\epsilon} = 10^{-3}$ s^{-1}	6.5 ±5.5 (6)	87.4 ±1.5 (5)	35.0 ±18.0 (4)
$\dot{\epsilon} = 10^{-5}$ s^{-1}	6.8 ±2.5 (4)	85.3 ±2.2 (4)	36.8 ±13.3 (4)
All samples	5.4 ±3.5 (39)	85.8 ±3.2 (33)	36.5 ±10.1 (38)

* Estimated angle between the load and mean c-axis direction.
† Unconfined compression test.
** Number of tests at those conditions.

measured σ:c angle of 16°. Using the Universal Stage we were also able to measure the angle between the columns or the direction of elongation of the crystals and the load direction (σ:z). Since all of our samples were taken in the plane of an undisturbed sheet of columnar first-year sea ice, σ:z was approximately 90°. The measured σ:c and σ:z angles for each sample are given in Appendix A.

Salinity, density and porosity

The salinity of each sample was measured after testing and after thin sections had been taken from

the sample. The tested specimen was cut into three sections (top, middle and bottom) and each section was melted in a separate container. The salinity in each container was measured with a conductance meter and the three values were averaged to give the sample salinity. The average salinity of all the horizontal samples used for testing was 3.70 $\pm 0.54‰$.

The sample densities were determined using simple mass/volume calculations. The average density of the tested samples at -10°C was 0.910 ± 0.007 Mg/m^3.

Porosities for each test specimen were also calculated from the salinity, density and test temperature (-10°C) of each sample using equations developed by Cox and Weeks (1983). The average porosity of the test specimens was 33.9 $\pm 7.9‰$.

The mean salinity, density and porosity for the samples grouped according to test condition are given in Table 3.

TEST RESULTS

Detailed results from the unconfined and confined constant-strain-rate compression tests are tabulated in Appendix A. Summaries of these results will be given in the following sections using tables and graphs. In the tables, σ_r/σ_a is the ratio between the radial confining pressure and the axial stress. This ratio was constant throughout the test. Note that the mean values in these tables and graphs do not account for any variation in the structural characteristics of the sample groups. As we will discuss below, our test results indicate that the mechanical behavior of a horizontal columnar sample is significantly influenced by its inherent structural characteristics. We will still use the mean value to describe many of the test results, however, since it does provide a reasonably accurate and convenient method of comparing the results between groups.

Strength

The mean strength of the samples grouped according to test conditions is summarized in Table 4. No strength is given at the test condition of $\sigma_r/\sigma_a = 0.75$, $\dot{\varepsilon} = 10^{-3}$ s^{-1} and σ:c angle of 0° because the 18.6-MPa (2700-lb/in.^{2}) capacity of the triaxial cell was exceeded in one-half of these tests. The influence of strain rate, c-axes orientation relative to the load (σ:c) and confinement is immediately evident. The compressive strength of the aligned, columnar samples is anisotropic in the plane of the ice sheet. Samples with an estimated σ:c angle of 0° have a greater strength than the samples with a σ:c angle of 90° and both are greater in strength than the 45° samples (0° samples > 90° samples > 45° samples). At each σ:c angle, there is an increase in strength with an increase in strain rate and an increase in radial confining pressure.

The mean compressive strength of the ice test specimens is plotted against strain rate in Figure 20. Each graph represents the results at a different estimated σ:c angle. Based on earlier work by Mellor (1983), we have assumed a power law relationship between the strength and strain rate from 10^{-1} to 10^{-5} s^{-1}. We can then describe the influence of strain rate using the equation $\sigma = A\,\dot{\varepsilon}^B$ (B, the slope of the line, is defined as the strain-rate sensitivity). Comparing the figures we observe that the strain-rate sensitivity varies between estimated σ:c angles but shows no dependency on confinement ratio.

This differs from observations made by Sinha (1985) in a series of laterally confined compression tests on second-year columnar-grained sea ice. Sinha reported a significant reduction in strain-rate sensitivity with confinement in these tests. The B-value for the unconfined 0° samples does agree well with the value of 0.32 reported by him (Sinha 1984) for unconfined tests at the same σ:c orientation (see Fig. 20a). Our unconfined strength values, however, are higher than those presented in Sinha's paper. These differences in test results may be attributable to variations in system stiffness, as described by Sinha and Frederking (1979), and to variations in sample preparation and test techniques. The compression tests performed by Sinha were done in the field on a conventional screw-driven machine with a design load capacity of 50 kN. This machine is soft relative to the testing system that we used in the laboratory. The influence of machine stiffness on the quality of test results becomes critical at higher strain rates and confining pressures where the ice becomes stiffest. In a soft machine under these conditions, we would expect the actual compressive strength of the ice to be reduced. On the other hand, the strength of the ice at the slower strain rate of 10^{-5} s^{-1} is not significantly affected by system stiffness. This variation in sensitivity to system stiffness would cause the strain-rate sensitivity, B, to become lower as confinement is applied to a sample in a relatively soft system. Note that the ice samples tested by Sinha also had an average salinity 1-2‰ higher than our samples.

Table 3. Mean salinity, density and porosity of first-year sea ice samples.

	Salinity (‰)	*Density* (Mg/m^3)	*Porosity* (‰)	*Number of samples*
		σ_r/σ_a = 0.0*		
$\dot{\epsilon} = 10^{-2}\ s^{-1}$				
45°	3.41 ± 0.88	0.910 ± 0.005	32.2 ± 9.2	4
$\dot{\epsilon} = 10^{-3}\ s^{-1}$				
0°	3.87 ± 0.62	0.914 ± 0.007	30.5 ± 10.0	4
90°	3.97 ± 0.97	0.913 ± 0.002	33.0 ± 6.5	4
45°	3.77 ± 0.43	0.904 ± 0.005	41.0 ± 7.3	6
$\dot{\epsilon} = 10^{-4}\ s^{-1}$				
0°	4.05 ± 0.59	0.914 ± 0.006	31.8 ± 5.2	4
90°	3.92 ± 0.70	0.913 ± 0.007	32.9 ± 8.2	4
45°	3.49 ± 0.56	0.908 ± 0.007	34.5 ± 3.2	4
		σ_r/σ_a = 0.25		
$\dot{\epsilon} = 10^{-3}\ s^{-1}$				
0°	3.87 ± 0.62	0.914 ± 0.007	30.5 ± 10.0	6
90°	3.97 ± 0.97	0.913 ± 0.002	33.0 ± 6.5	4
45°	3.77 ± 0.43	0.904 ± 0.005	41.0 ± 7.3	4
$\dot{\epsilon} = 10^{-4}\ s^{-1}$				
0°	4.64 ± 0.95	0.909 ± 0.008	37.5 ± 10.0	7
90°	3.80 ± 0.57	0.919 ± 0.012	32.7 ± 9.0	4
45°	3.93 ± 0.69	0.916 ± 0.005	29.4 ± 9.3	4
		σ_r/σ_a = 0.50		
$\dot{\epsilon} = 10^{-4}\ s^{-1}$				
0°	3.39 ± 0.45	0.910 ± 0.003	31.9 ± 3.8	4
90°	3.57 ± 0.34	0.912 ± 0.001	31.2 ± 1.4	4
45°	3.81 ± 0.29	0.913 ± 0.003	32.6 ± 2.6	4
$\dot{\epsilon} = 10^{-5}\ s^{-1}$				
0°	3.60 ± 0.29	0.911 ± 0.002	32.8 ± 0.4	4
90°	3.60 ± 0.57	0.912 ± 0.001	31.5 ± 3.6	4
45°	3.79 ± 0.20	0.894 ± 0.014	52.6 ± 16.4	4
		σ_r/σ_a = 0.75		
$\dot{\epsilon} = 10^{-4}\ s^{-1}$				
0°	3.43 ± 0.44	0.911 ± 0.002	31.7 ± 3.8	6
90°	3.28 ± 0.57	0.909 ± 0.003	32.5 ± 6.4	5
45°	3.51 ± 0.41	0.906 ± 0.004	37.2 ± 4.69	4
$\dot{\epsilon} = 10^{-5}\ s^{-1}$				
0°	3.47 ± 0.39	0.916 ± 0.002	26.9 ± 4.0	4
90°	3.53 ± 0.43	0.911 ± 0.001	32.6 ± 2.4	4
45°	3.82 ± 0.26	0.911 ± 0.002	34.5 ± 1.1	4
All samples	3.70 ± 0.54	0.911 ± 0.007	33.9 ± 7.9	110

* Unconfined compression test

Table 4. Mean compressive strength of horizontal samples of columnar first-year sea ice (test temperature = -10°C).

	σ:c*					
	0°		90°		45°	
	(MPa)	(lbf/in.²)	(MPa)	(lbf/in.²)	(MPa)	(lbf/in.²)
			σ_r/σ_a = 0.0†			
$\dot{\epsilon}$ = 10^{-2} s^{-1}	—	—	—	—	4.63 ± 1.59	671 ± 230 (4)**
$\dot{\epsilon}$ = 10^{-3} s^{-1}	7.30 ± 1.91	1058 ± 277 (4)	6.56 ± 1.88	951 ± 273 (4)	4.27 ± 0.83	619 ± 120 (4)
$\dot{\epsilon}$ = 10^{-5} s^{-1}	1.59 ± 0.50	230 ± 72 (4)	1.50 ± 0.45	218 ± 65 (4)	0.59 ± 0.03	86 ± 5 (4)
			σ_r/σ_a = 0.25			
$\dot{\epsilon}$ = 10^{-3} s^{-1}	12.52 ± 4.64	1816 ± 673 (6)	9.89 ± 0.29	1434 ± 303 (4)	7.01 ± 0.80	1016 ± 116 (4)
$\dot{\epsilon}$ = 10^{-5} s^{-1}	2.11 ± 0.52	306 ± 76 (7)	1.37 ± 0.13	198 ± 19 (4)	1.01 ± 0.07	146 ± 10 (4)
			σ_r/σ_a = 0.50			
$\dot{\epsilon}$ = 10^{-3} s^{-1}	17.41 ± 4.86	2524 ± 705 (4)	15.37 ± 0.48	2228 ± 70 (4)	11.19 ± 1.72	1623 ± 249 (4)
$\dot{\epsilon}$ = 10^{-5} s^{-1}	3.15 ± 1.19	457 ± 172 (4)	3.50 ± 0.64	507 ± 93 (4)	1.16 ± 0.26	168 ± 38 (4)
			σ_r/σ_a = 0.75			
$\dot{\epsilon}$ = 10^{-3} s^{-1}	—	—	26.79 ± 2.32	3739 ± 337 (3)	16.41 ± 5.13	2379 ± 744 (4)
$\dot{\epsilon}$ = 10^{-5} s^{-1}	8.22 ± 1.70	1192 ± 247 (4)	7.00 ± 2.46	1015 ± 356 (4)	3.50 ± 1.49	507 ± 216 (4)

* Estimated angle between the load and mean c-axis direction.

† Unconfined compression test.

** Number of samples used to determine the mean and standard deviation.

In the unconfined tests on the 45° samples, shown in Figure 20c, there was an 8% increase in mean compressive strength with an increase in strain rate between 10^{-3} and 10^{-2} s^{-1}. Results from tests done at CRREL on multi-year ridge ice samples (Cox et al. 1985) indicate a leveling off of strength between 10^{-3} and 10^{-2} s^{-1}. Work by Bohon and Weingarten (1985) of Arco Oil and Gas Company suggests that the unconfined compressive strength of ice increases with strain rate up to 2×10^{-3} s^{-1}. After reaching this peak, the strength in their tests drops off rapidly. Work is currently underway at both CRREL and Arco to determine which data set correctly describes the strength behavior of ice in the brittle region.

The compressive strength of each test specimen is plotted against the *actual* σ:c angle in Figure 21. The actual σ:c angle was measured in the laboratory on the Rigsby Universal Stage using thin sections from each tested sample. The numbers given next to each data point represent, first, the core hole from which the sample was taken and, second, the depth of the horizontal sample from the top of the ice sheet in centimetres. In Figure 21a, we have combbned the 10^{-3} and 10^{-2} s^{-1} test results for the unconfined compression tests.

The unconfined compressive strengths of the horizontal samples agree very well with results presented by Wang (1979a) at a strain rate of 10^{-3} s^{-1} and test temperature of -10°C (see Fig. 21a).

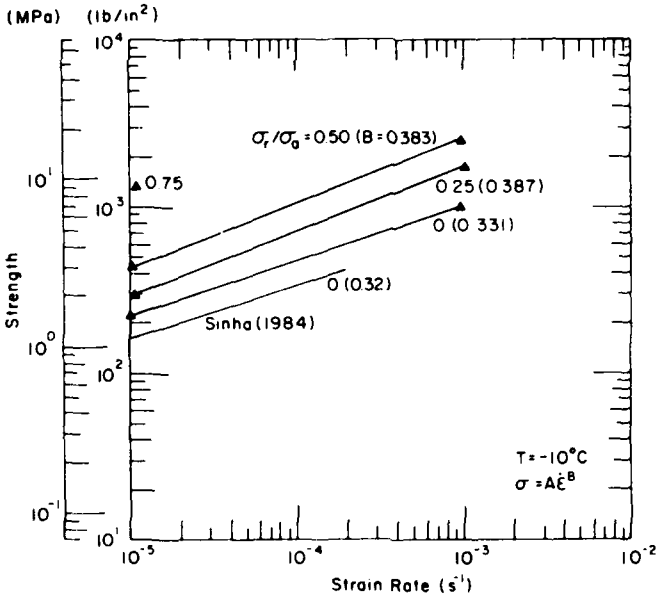

a. Estimated σ:c angle of 0°.

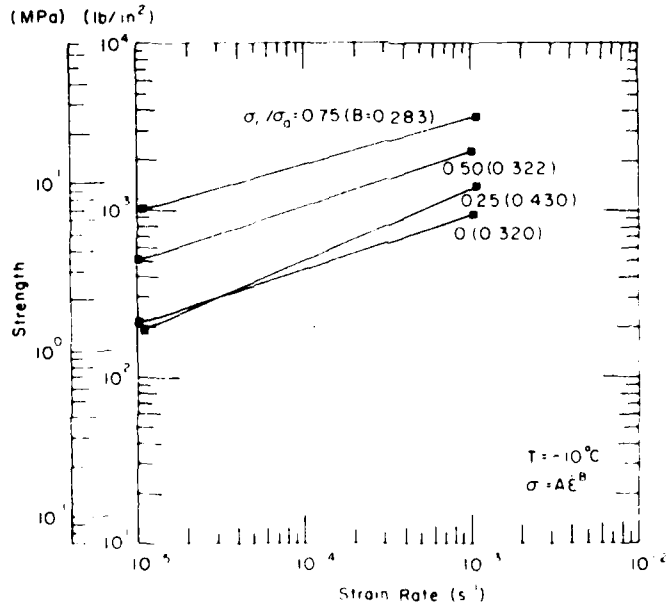

b. Estimated σ:c angle of 90°.

Figure 20. Mean compressive strength of first-year sea ice samples vs strain rate.

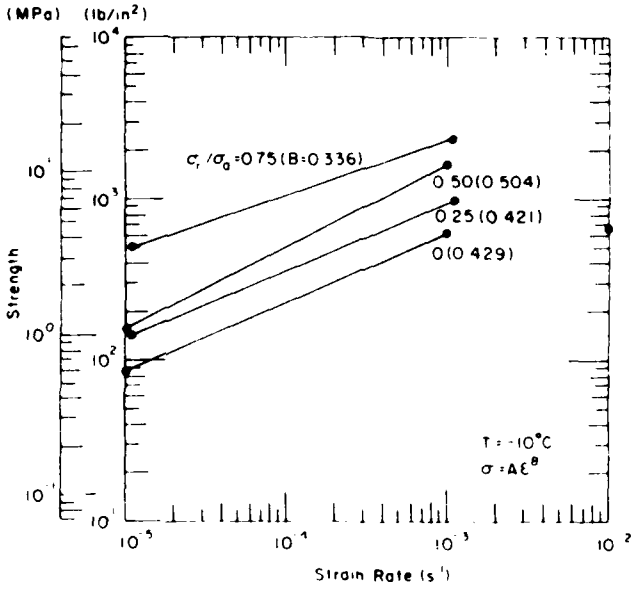

c. Estimated σ:c angle of 45°.

Figure 20 (cont'd).

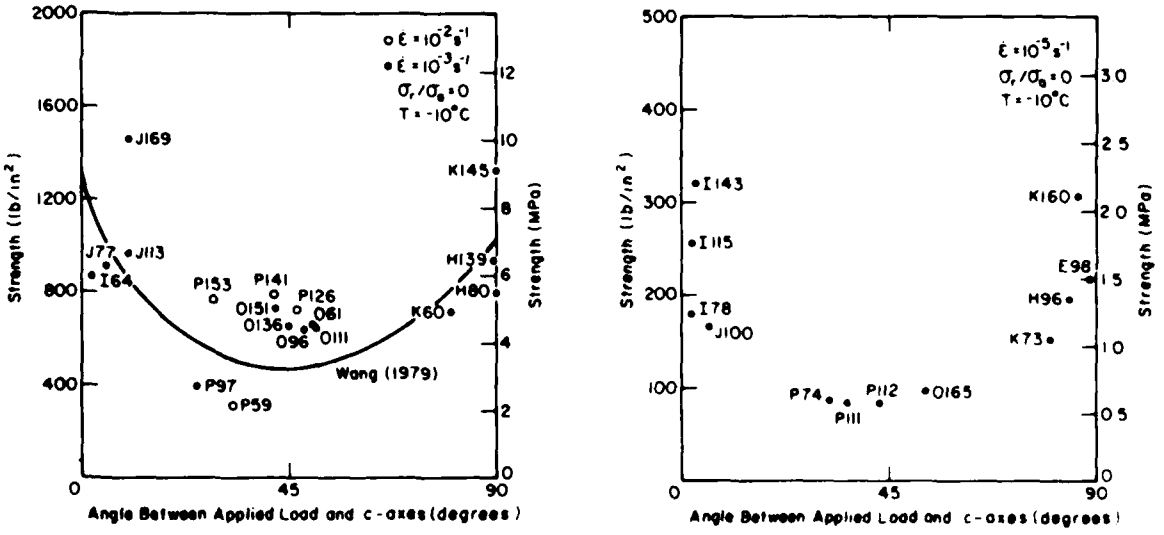

a. Tests conducted at 10^{-3} and 10^{-2} s^{-1} and $\sigma_r/\sigma_a = 0$.

b. Tests conducted at 10^{-5} s^{-1} and $\sigma_r/\sigma_a = 0$.

Figure 21. Compressive strength of first-year sea ice samples vs angle between applied load and crystal c-axes. The letter representing the core hole and the depth (cm) below the top of the ice sheet of each sample is given next to the data point.

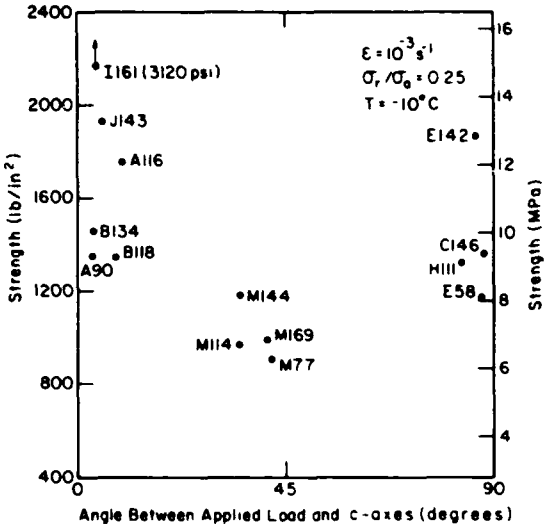

c. Tests conducted at 10^{-3} s^{-1} and σ_r/σ_a = 0.25.

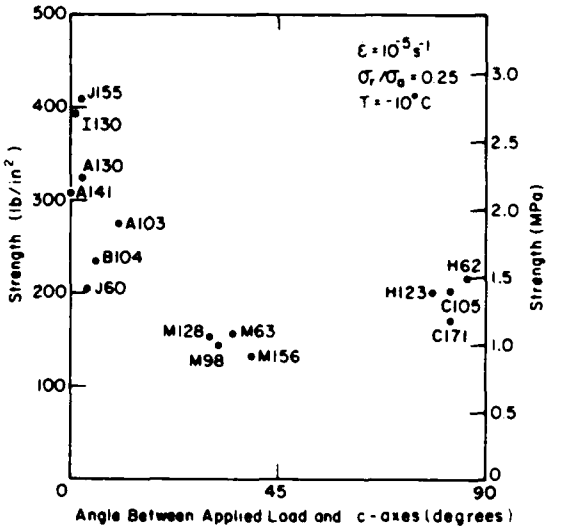

d. Tests conducted at 10^{-5} s^{-1} and σ_r/σ_a = 0.25.

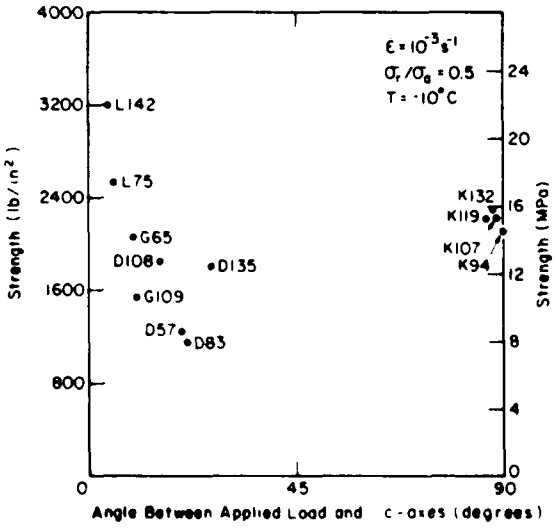

e. Tests conducted at 10^{-3} s^{-1} and σ_r/σ_a = 0.50.

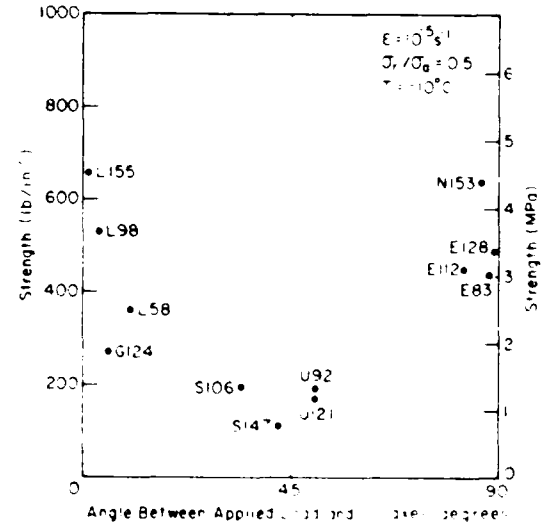

f. Tests conducted at 10^{-5} s^{-1} and σ_r/σ_a = 0.50.

Figure 21 (cont'd). Compressive strength of first-year sea ice samples vs angle between applied load and crystal c-axes. The letter representing the core hole and the depth (cm) below the top of the ice sheet of each sample is given next to the data point.

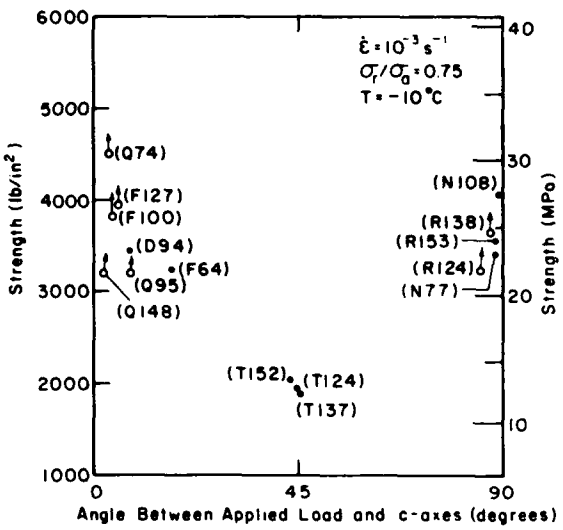

g. Tests conducted at 10^{-3} s^{-1} and $\sigma_r/\sigma_a = 0.75$.

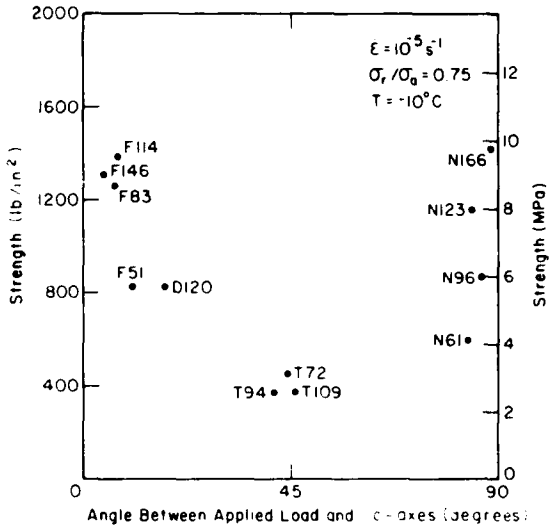

h. Tests conducted at 10^{-5} s^{-1} and $\sigma_r/\sigma_a = 0.75$.

Figure 21 (cont'd).

The tests by Wang were also conducted in the laboratory on a closed-loop, electrohydraulic testing machine. The strength distribution with respect to measured σ:c angle of our test results does tend to be more U-shaped than the distribution shown by Wang in Figure 21a. In other words, our tests show a significant variation in compressive strength at σ:c angles of 0° and 90°. This may be ascribable to the surprisingly large increase in compressive strength of the 0° and 90° samples with depth that is apparent at all of our test conditions. One extreme example is given in Figure 21c where two 0° samples from 143 and 161 cm depths have respective strengths of 12.62 and 21.56 MPa. While we attribute some of this increase in strength to the increase in the degree of alignment of the c-axes in the horizontal plane with increasing depth, we do not feel that this factor alone can account for the magnitude of the change. Other characteristic changes in the columnar first-year ice sheet that coincide with depth must also be considered. These include the increase in spacing between brine layers with depth, systematic changes in the distribution of brine channels, and variations in the salinity, brine volume and grain size. More work needs to be done to define the variation in strength with each of these parameters.

As we mentioned earlier, the results of our tests indicate that the compressive strength of the 0° samples is greater than that of the 90° samples which is greater than that of the 45° samples regardless of confinement ratio. This supports observations made in unconfined compression tests performed by Wang (1979a,b) and Peyton (1966). Sinha (1985), however, reported no variation in strength with the σ:c angle under directionally confined loading conditions. In Sinha's tests, the columnar ice deformation was restricted in the plane of the ice sheet. Consequently, the orientation of the c-axes, which also lie in the plane of the ice sheet, no longer has a significant influence on the strength. Ratios of the mean compressive strength between samples grouped according to the estimated σ:c values of 0°, 90° and 45° are presented in Table 5. The ratios obtained by Peyton and Wang are also included for comparison. In general, the results from our tests tend to give lower strength ratios between σ:c groups. This is not surprising, however, since our samples vary significantly both in degree of c-axes alignment and actual σ:c angles (Appendix A). Both Wang and Peyton used only strongly aligned columnar samples in their tests.

Table 5. Ratio of mean compressive strength between estimated σ:c angle groups of horizontal samples of columnar first-year sea ice (test temperature = -10°C).

	0°:90°	0°:45°	90°:45°
	σ_t/σ_a = 0.0*		
$\dot{\varepsilon} = 10^{-2}\ s^{-1}$	—	—	—
$\dot{\varepsilon} = 10^{-3}\ s^{-1}$	1.11	1.71	1.54
$\dot{\varepsilon} = 10^{-4}\ s^{-1}$	1.07	2.67	2.53
	σ_t/σ_a = 0.25		
$\dot{\varepsilon} = 10^{-3}\ s^{-1}$	1.27	1.79	1.41
$\dot{\varepsilon} = 10^{-4}\ s^{-1}$	1.55	2.10	1.36
	σ_t/σ_a = 0.50		
$\dot{\varepsilon} = 10^{-3}\ s^{-1}$	1.37	1.56	1.31
$\dot{\varepsilon} = 10^{-4}\ s^{-1}$	0.852	2.72	3.19
	σ_t/σ_a = 0.75		
$\dot{\varepsilon} = 10^{-3}\ s^{-1}$	—	—	1.57
$\dot{\varepsilon} = 10^{-4}\ s^{-1}$	1.32	2.64	2.00
Wang (1979b)	1.30	2.79	2.15
Peyton (1966)	1.67	3.94	2.36

* Unconfined compression test.

At all test conditions, regardless of the σ:c angle, the deformation characteristics of the compression samples were anisotropic. As observed in another work by Wang (1981), most of the deformation took place perpendicular to the direction of crystal elongation or in the plane of the ice sheet. Field tests done by Timco and Frederking (1983) and Blanchet and Hamza (1983) on prismodial samples also indicate that a sample subject to compression will deform in the plane of the ice sheet unless it is preferentially restrained from movement in that direction. Photographs of our samples after testing clearly illustrate this behavior. In Figure 22, a 0° sample is shown after testing in two mutually perpendicular positions. Figures 22a and b show the deformation perpendicular (in the plane of the ice sheet) and parallel (normal the plane of the ice sheet) to the crystal elongation direction respectively. The preferred direction of deformation is obvious.

The mean deviatoric strength (σ_1-σ_3) of the horizontal columnar samples for each test condition is plotted against the confining pressure ($\sigma_2 = \sigma_3$) at failure in Figure 23. Results from Hausler (1982) on unaligned, columnar saline samples grown in the laboratory are included for comparison. With respect to Hausler's work, we only used data from the tests that were loaded in the horizontal plane with $\sigma_1 > \sigma_2 = \sigma_3$. This corresponded to the loading state of our samples. Hausler's tests were conducted at a constant strain rate of $2 \times 10^{-4}\ s^{-1}$ and T = -10°C on cubic samples using brush-type loading platens. The samples used by Hausler had an average salinity of 10.6‰.

The shape of the yield surfaces for the first-year sea ice samples, shown in Figure 23, closely follows the yield surface as defined by Hausler's tests. In a subsequent paper Hausler (1983) has shown that this yield behavior can be well described by a Smith yield function. The general shape of the deviatoric strength distribution at both strain rates also agrees well with results presented by Jones (1982) on the confined compressive strength of freshwater polycrystalline ice at strain rates between 10^{-3} and $10^{-5}\ s^{-1}$. There is an initial increase in deviatoric strength with an increase in confining pressure, a peak or maximum is reached and then the deviatoric strength begins

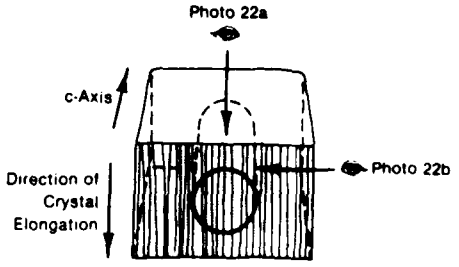

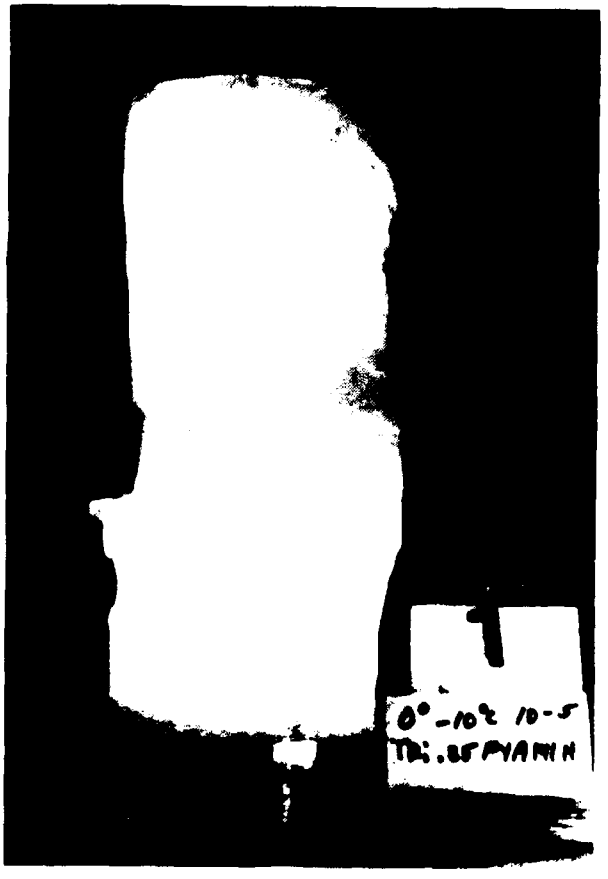

a. Deformation in the plane of ice sheet or perpendicular to direction of crystal elongation.

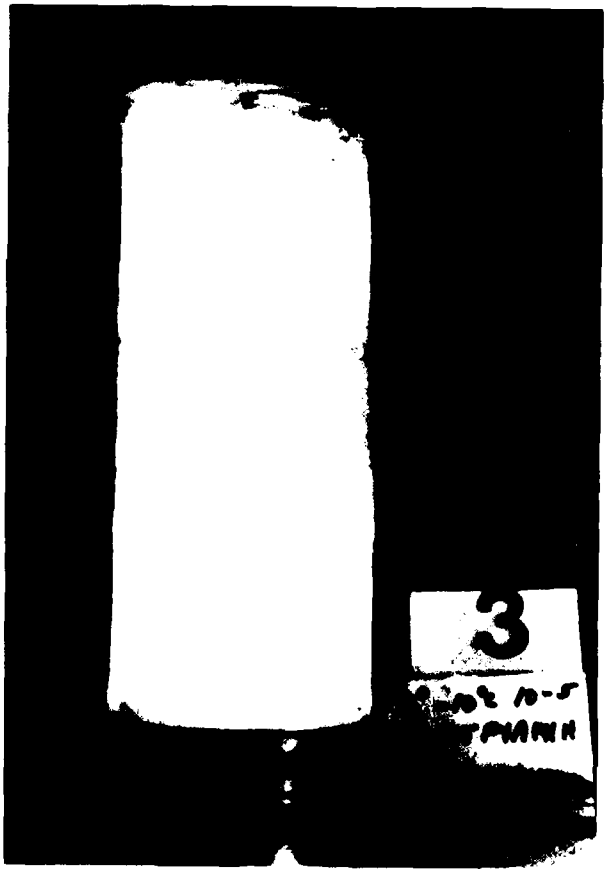

b. Deformation normal to plane of ice sheet or parallel to direction of crystal elongation.

Figure 22. Deformation of a tested specimen both perpendicular and parallel to the direction of crystal elongation ($\dot{\epsilon} = 10^{-5}\ s^{-1}$, $T = -10\ C$, $\sigma_r / \sigma_a = 0.25$ and estimated c-c angle of 0°).

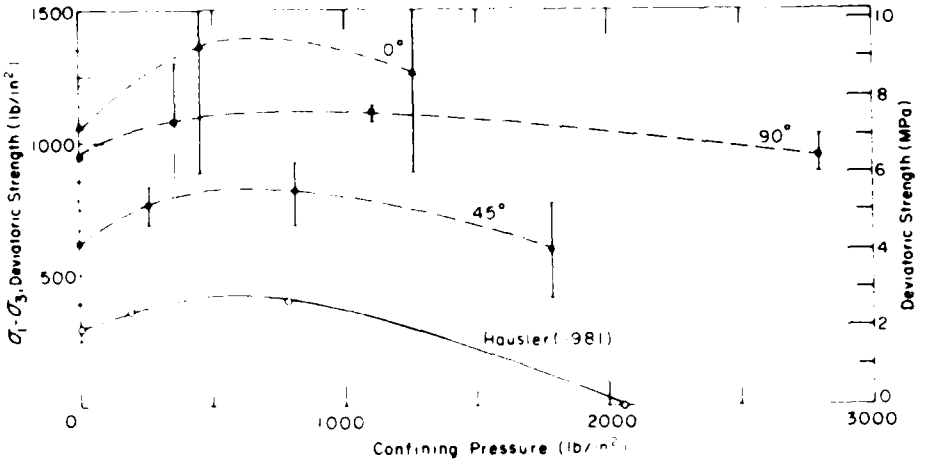

a. Tests conducted at 10^{-1} s^{-1}.

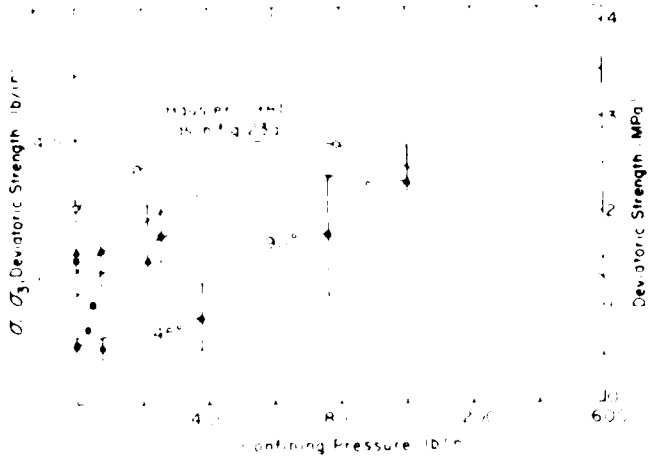

b. Test conducted at 10^{-4} s^{-1}.

Figure 23. Mean deviatoric strength of first-year sea ice samples vs confining pressure at failure. The test temperature is -10°C.

to decrease. The maximum deviatoric strength in the higher-strain-rate tests (Fig. 23a), however, occurs at a much lower confining pressure than in Jones' tests. Note that even at the lower strain rate of 10^{-4} s^{-1} (Fig. 23b) the deviatoric strength of the first-year ice is increasing slightly with an increase in confining pressure. This suggests that the columnar ice does not strictly behave as a Tresca or Von Mises material even at these conditions where the ice is behaving in a ductile manner. A similar observation has been made by Panov and Fokeev (1977).

The influences of confinement, structure and strain rate are collectively seen in the characteristics of the stress-strain curves. In Table 6 and Figure 24 we have defined the four typical stress-strain curves observed in our tests. In the unconfined compression tests at strain rates of 10^{-2} and 10^{-4} s^{-1}, many of the tests exhibited brittle-type failure (type A) while at 10^{-6} s^{-1} all of the samples reached a pronounced maximum stress, underwent strain-softening and then plastic flow (type B). A confinement ratio of 0.25 was adequate to suppress brittle failure at 10^{-4} s^{-1} and the tests ex-

Table 6. Characteristic stress–strain curves of horizontal samples of first-year sea ice (test temperature = −10°C).

	σ:c*		
	0°	90°	45°
	σ_r/σ_a = 0.0†		
$\dot{\epsilon} = 10^{-2}$ s^{-1}	—	—	A**
$\dot{\epsilon} = 10^{-3}$ s^{-1}	A&B	A&B	A
$\dot{\epsilon} = 10^{-4}$ s^{-1}	B	B	B
	σ_r/σ_a = 0.25		
$\dot{\epsilon} = 10^{-3}$ s^{-1}	B	B	B
$\dot{\epsilon} = 10^{-4}$ s^{-1}	B	B	B
	σ_r/σ_a = 0.50		
$\dot{\epsilon} = 10^{-3}$ s^{-1}	B	B	B
$\dot{\epsilon} = 10^{-4}$ s^{-1}	B&D	B	B&D
	σ_r/σ_a = 0.75		
$\dot{\epsilon} = 10^{-3}$ s^{-1}	B&C	B&C	B&C
$\dot{\epsilon} = 10^{-4}$ s^{-1}	B&D	B&C	D

* Estimated angle between the load and mean c-axis direction.

† Unconfined compression test.

** See Figure 24.

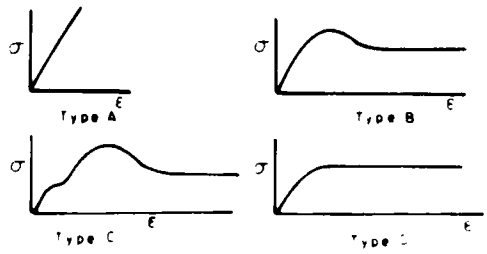

Figure 24. Characteristic stress–strain curves of horizontal samples of first-year sea ice.

hibited the type B characteristics mentioned above. The next significant change in behavior took place at σ_r/σ_a = 0.50 and a strain rate of 10^{-4} s^{-1} when the stress–strain curves became very flat (type D), indicating a high degree of plasticity. Although this behavior was never observed at a strain rate of 10^{-3} s^{-1}, some of the high rate tests at σ_r/σ_a = 0.75 did exhibit an initial yield point (type C). In general, the degree of ductility increased with an increase in confinement.

Failure strains

The compressive strength of each test specimen is plotted against the corresponding strain at failure in Figure 25. Each plot represents a different confinement ratio. There is a tendency for the failure strain to increase with an increase in strength and confinement at a given strain rate. The range of failure strains between the 10^{-3} and 10^{-4} s^{-1} strain-rate tests at a given confinement ratio overlap. In the unconfined tests on the 45°

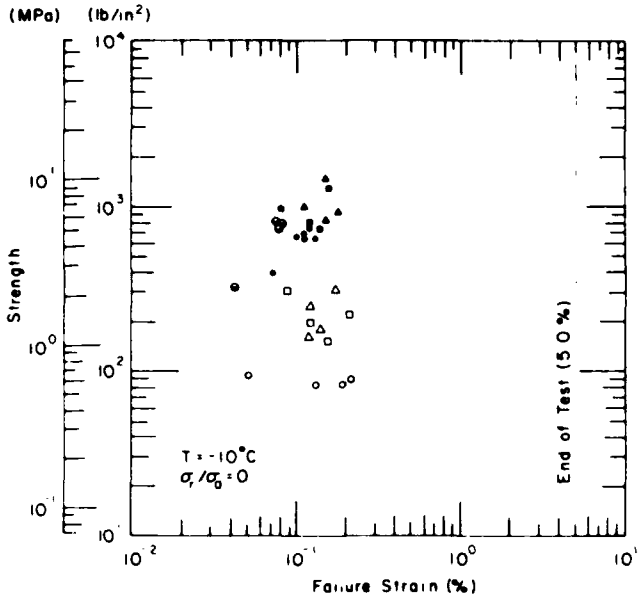

σ : C / $\dot{\varepsilon}$	$10^{-2}s^{-1}$	$10^{-3}s^{-1}$	$10^{-5}s^{-1}$
0°		▲	△
90°		■	□
45°	●	●	○

a. Tests conducted at $\sigma_r/\sigma_a = 0$.

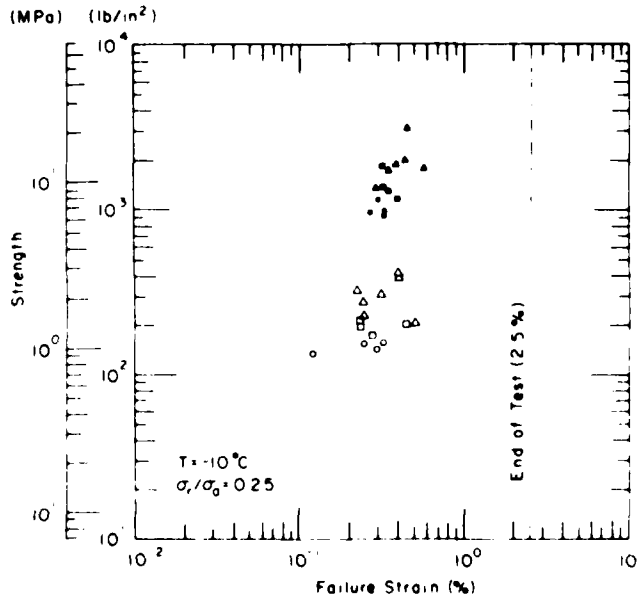

σ : C / $\dot{\varepsilon}$	$10^{-2}s^{-1}$	$10^{-3}s^{-1}$	$10^{-5}s^{-1}$
0°		▲	△
90°		■	□
45°	●	●	○

b. Tests conducted at $\sigma_r/\sigma_a = 0.25$.

Figure 25. Compressive strength of first-year sea ice samples vs strain at failure. The test temperature is -10°C unless otherwise noted.

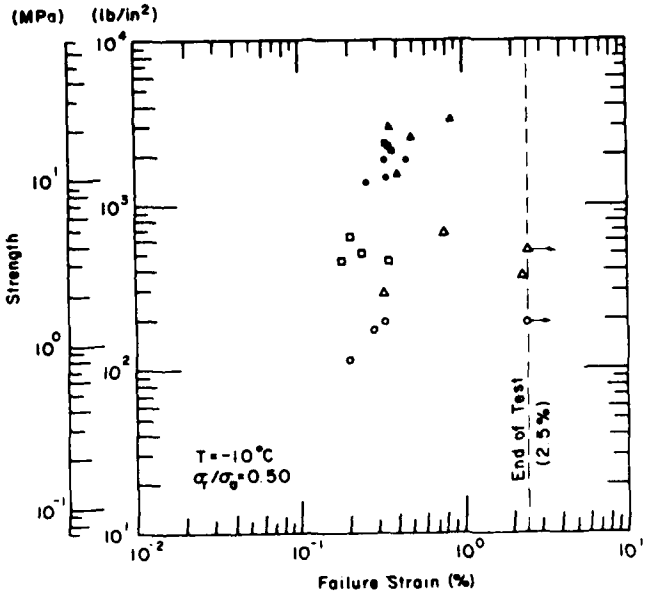

σ:C	10^{-2}s^{-1}	10^{-3}s^{-1}	10^{-5}s^{-1}
0°		▲	△
90°		●	□
45°	●	●	○

c. Tests conducted at σ_r/σ_a = 0.50.

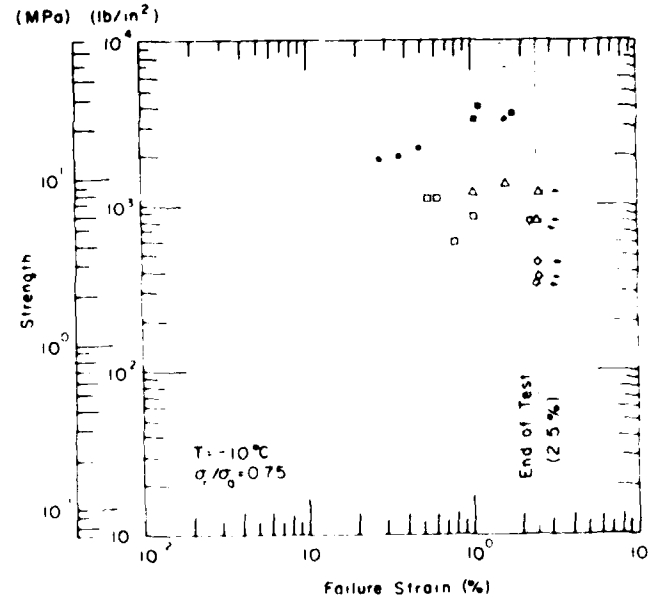

σ:C	10^{-2}s^{-1}	10^{-3}s^{-1}	10^{-5}s^{-1}
0°		▲	△
90°		●	□
45°	●	●	○

d. Tests conducted at σ_r/σ_a = 0.75.

Figure 25 (cont'd).

Table 7. Mean axial strain at failure (%) for horizontal samples of columnar first-year sea ice (test temperature = -10°C).

	σ:c*		
	0°	90°	45°
	σ_r/σ_a = 0.0†		
$\dot{\epsilon} = 10^{-2}$ s^{-1}	—	—	0.069 ±0.018 (4)**
$\dot{\epsilon} = 10^{-3}$ s^{-1}	0.147 ±0.029 (4)	0.125 ±0.034 (4)	0.107 ±0.021 (6)
$\dot{\epsilon} = 10^{-4}$ s^{-1}	0.137 ±0.030 (4)	0.141 ±0.053 (4)	0.142 ±0.070 (4)
	σ_r/σ_a = 0.25		
$\dot{\epsilon} = 10^{-3}$ s^{-1}	0.462 ±0.087 (6)	0.382 ±0.071 (4)	0.307 ±0.029 (4)
$\dot{\epsilon} = 10^{-4}$ s^{-1}	0.311 ±0.094 (7)	0.292 ±0.100 (4)	0.245 ±0.088 (4)
	σ_r/σ_a = 0.50		
$\dot{\epsilon} = 10^{-3}$ s^{-1}	0.522 ±0.225 (4)	0.350 ±0.008 (4)	0.370 ±0.125 (4)
$\dot{\epsilon} = 10^{-4}$ s^{-1}	1.130 ±1.045 (3)	0.242 ±0.076 (4)	0.277 ±0.071 (3)
	σ_r/σ_a = 0.75		
$\dot{\epsilon} = 10^{-3}$ s^{-1}	0.75 (1)	1.287 ±0.384 (3)	0.667 ±0.581 (4)
$\dot{\epsilon} = 10^{-4}$ s^{-1}	1.32 ±0.48 (2)	0.742 ±0.22 (4)	—

* Estimated angle between the load and the mean c-axis direction.
† Unconfined compression test.
** Number of samples used to determine the mean and standard deviation.

samples, the range of failure strains decreased with an increase in strain rate between 10^{-1} and 10^{-2} s^{-1}. In general, the values of the failure strains in the unconfined tests agree well with strains measured by Hausler (1981), but are slightly lower than those measured by Sinha (1984) and Frederking and Timco (1983). This may again be attributed to the softer testing machines used by both Sinha and Frederking and Timco in their field tests. The failure strains in the confined compression tests agree well with measurements made by Cox et al. (1985) on samples of multi-year ridge sea ice. The mean strain at failure is summarized in Table 7.

Initial tangent modulus

We estimated the initial tangent modulus ($\Delta\sigma_i/\Delta\epsilon_i$) of each horizontal columnar sample from the initial linear slope of the force-displacement curve for each compression test. In most test cases this linear portion of the curve extended to a minimum of 25% of the yield stress. Axial displacement was determined from the average displacement of the DCDTs mounted on the sample for the unconfined tests. A pair of LVDTs mounted on the sample end caps was used to make the displacement measurements in the confined tests.

Table 8. Mean initial tangent modulus of horizontal samples of columnar first-year sea ice (test temperature = -10°C).

	σ:c*					
	0°		90°		45°	
	(GPa)	(10^4 lbf/in.^{2})	(GPa)	(10^4 lbf/in.^{2})	(GPa)	(10^4 lbf/in.^{2})
			σ_r/σ_a = 0.0†			
$\dot{\epsilon}$ = 10^{-2} s^{-1}	—	—	—	—	7.28 ±0.67	1.056 ±0.097 (4)
$\dot{\epsilon}$ = 10^{-3} s^{-1}	8.39 ±1.25	1.216 ±0.182 (4)	7.92 ±1.19	1.149 ±0.172 (4)	8.26 ±1.78	1.197 ±0.258 (6)
$\dot{\epsilon}$ = 10^{-4} s^{-1}	7.92 ±1.49	1.149 ±0.216 (4)	4.88 ±0.62	0.708 ±0.090 (4)	4.12 ±1.08	0.597 ±0.157 (4)
			σ_r/σ_a = 0.25			
$\dot{\epsilon}$ = 10^{-3} s^{-1}	6.36 ±0.43	0.922 ±0.062 (3)	6.58	0.954 (1)	—	—
$\dot{\epsilon}$ = 10^{-4} s^{-1}	6.23	0.903 (1)	—	—	—	—
			σ_r/σ_a = 0.50			
$\dot{\epsilon}$ = 10^{-3} s^{-1}	7.97 ±1.18	1.156 ±0.171 (4)	8.34 ±0.55	1.209 ±0.080 (4)	7.48 ±1.31	1.084 ±0.190 (4)
$\dot{\epsilon}$ = 10^{-4} s^{-1}	5.79 ±1.54	0.840 ±0.224 (4)	6.54 ±1.50	0.949 ±0.218 (4)	4.68 ±0.71	0.678 ±0.103 (4)
			σ_r/σ_a = 0.75			
$\dot{\epsilon}$ = 10^{-3} s^{-1}	10.34 ±0.58	1.500 ±0.084 (5)	10.24 ±0.81	1.458 ±0.118 (5)	8.66 ±0.70	1.255 ±0.102 (5)
$\dot{\epsilon}$ = 10^{-4} s^{-1}	8.61 ±1.59	1.249 ±0.230 (4)	11.50 ±1.73	1.667 ±0.251 (4)	6.74 ±0.30	0.978 ±0.044 (4)

* Estimated angle between the load and the mean c-axis direction.

† Unconfined compression test.

** Number of samples used to determine the mean and standard deviation.

A summary of the mean initial tangent modulus values for each test condition is given in Table 8. The results show that the modulus increased with an increase in strain rate at each confinement ratio. This supports observations made by Traetteberg et al. (1975) in tests on laboratory-grown freshwater granular and columnar ice samples, and by Cox et al. (1984, 1985) in tests on multiyear ridge ice samples. In the confined compression tests the modulus also increased with an increase in confinement ratio at both strain rates. The mean initial tangent modulus was still slightly higher in the unconfined tests than in the confined tests with σ_r/σ_a = 0.25. This is probably due to the change in location of the transducers measuring the axial displacement between the unconfined and confined tests. While the full sample and gauge length strain measurements show close agreement in the unconfined test results, there is still a tendency for the full sample strains to be greater than the gauge length strains. Consequently, the full sample strain measurements used in the confined tests would result in a slightly lower initial modulus tangent.

CONCLUSIONS

Unconfined and confined constant strain rate compression tests were performed on horizontal

samples of columnar first-year sea ice from the Beaufort Sea. All of the samples exhibited alignment of the crystallographic c-axes in the horizontal plane of the ice sheet. The test techniques that we used in this investigation were originally developed for a program involving tests on multi-year pressure ridge ice samples. Modifications were made to the conventional triaxial cell to obtain more accurate initial tangent modulus, strain and strain-rate measurements.

The results indicate that the anisotropic behavior of the ice in the horizontal plane exists both under confined and unconfined test conditions. This is reflected both in the strength and deformation characteristics of the tested specimen. A sample loaded parallel to the direction of the aligned c-axes has a higher strength than a sample loaded perpendicular to the c-axes. As the angle between the load and the c-axes direction approaches 45°, the strength reaches a minimum. Deformation mainly occurs in the plane of the ice sheet that is normal to the direction of crystal elongation. The strength at all orientations increases with an increase in confinement, as does the strain at failure and the initial tangent modulus. For samples loaded parallel and perpendicular to the c-axes direction, there is also a significant increase in strength with an increase in depth. At an angle of 45° between the load and c-axes direction, the strength is independent of depth.

LITERATURE CITED

Blanchet, D. and H. Hamza (1983) Plane-strain compressive strength of first-year Beaufort Sea ice. *Proceedings of the 7th International Conference on Port and Ocean Engineering Under Arctic Conditions (POAC '83), 5-9 April, Helsinki, Finland.* Vol. 3, pp. 84-96.

Bohon, W.M. and J.S. Weingarten (1985) The calculation of ice forces on arctic structures. *Proceedings, ASCE Arctic '85 Conference, 25-27 March, Dallas, Texas.* New York: American Society of Civil Engineers, pp. 456-464.

Cole, D.M., L.D. Gould and W.B. Burch (1986) A system for mounting end caps on ice specimens. *Journal of Glaciology*, **31**(109): 362-365.

Cox, G.F.N. and J.A. Richter-Menge (1985) Triaxial compression testing of ice. *Proceedings, ASCE Arctic '85 Conference, 25-27 March, Dallas, Texas.* New York: American Society of Civil Engineers, pp. 476-488.

Cox, G.F.N. and W.F. Weeks (1983) Equations for determining the gas and brine volumes in sea ice samples. *Journal of Glaciology*, **29**(2): 306-316.

Cox, G.F.N., J.A. Richter-Menge, W.F. Weeks, M. Mellor, and H.W. Bosworth (1984) Mechanical properties of multi-year sea ice, Phase I: Test results. USA Cold Regions Research and Engineering Laboratory, CRREL Report 84-9.

Cox, G.F.N., J.A. Richter-Menge, W.F. Weeks, M. Mellor, H.W. Bosworth, G. Durell and N. Perron (1985) The mechanical properties of multi-year sea ice, Phase II: Test results. USA Cold Regions Research and Engineering Laboratory, CRREL Report 85-16.

Frederking, R. and G.W. Timco (1983) Uniaxial compressive strength and deformation of Beaufort Sea ice. *Proceedings of the 7th International Conference on Port and Ocean Engineering Under Arctic Conditions (POAC '83), 5-9 April, Helsinki, Finland.* Vol. 1, pp. 89-98.

Gow, A.J. and W.F. Weeks (1977) The internal structure of fast ice near Narwhal Island, Beaufort Sea, Alaska. USA Cold Regions Research and Engineering Laboratory, CRREL Report 77-29.

Hausler, F.U. (1983) Comparison between different yield functions for saline ice. *International Glaciological Society, Annals of Glaciology*, **4**: 105-109.

Hausler, F.U. (1981) Multiaxial compressive strength tests on saline ice with brush-type loading platens. *Proceedings of the International Association for Hydraulic Research, International Symposium on Ice, 27-31 July, Quebec, Canada.* Vol. 2, pp. 526-539.

Hawkes, I. and M. Mellor (1972) Deformation and fracture of ice under uniaxial stress. *Journal of Glaciology*, **11**(61): 103-131.

Jones, S.J. (1982) The confined compressive strength of polycrystalline ice. *Journal of Glaciology*, **28**(98): 171-177.

Langway, C.C. (1958) Ice fabric and the universal stage. USA Snow, Ice and Permafrost Research Establishment, SIPRE Technical Report 62. (Available from USA Cold Regions Research and Engineering Laboratory, Hanover, New Hampshire.)

Larsen, L. (1980) Sediment-laden sea ice: Concepts, problems, and approaches. Outer Continental Shelf Environmental Assessment Program. Special Bulletin No. 29 (Donald M. Schell, Ed.), pp. 59-71.

Martin, S. (1981) Frazil ice in rivers and oceans. *Annual Review of Fluid Mechanics*, **13**: 379-397.

Mellor, M. (1983) Mechanical behavior of sea ice. USA Cold Regions Research and Engineering Laboratory, Monograph 83-1.

Mellor, M., G.F.N. Cox, and H.W. Bosworth (1984) Mechanical properties of multi-year sea ice: Testing techniques. USA Cold Regions Research and Engineering Laboratory, CRREL Report 84-8.

Nakawo, M. and N.K. Sinha (1981) Growth rate and salinity profile of first-year sea ice in the high Arctic. *Journal of Glaciology*, **27**(96): 315-330.

Nawwar, A.M., J.P. Nadreau and Y.S. Wang (1983) Triaxial compressive strength of saline ice. *Proceedings of the 7th International Conference on Port and Ocean Engineering under Arctic Conditions (POAC '83), 5-9 April, Helsinki, Finland.* Vol. 3, pp. 193-202.

Panov, V.V. and N.V. Fokeev (1977) Compressive strength of sea ice specimens under complex loading. *Promlemy Arktiki i Antarktiki*, **49**: 81-86 (English translation, pp. 97-104).

Peyton, H.R. (1966) Sea ice strength. Geophysical Institute, University of Alaska, Report UAG-182.

Rand, J. and M. Mellor (1985) Ice-coring augers for shallow depth sampling. USA Cold Regions Research and Engineering Laboratory, CRREL Report 85-21.

Richter-Menge, J.A. (1984) Static determination of Young's modulus in sea ice. *Cold Regions Science and Technology*, **9**(3): 283,286.

Schwarz, J., R. Frederking, V. Gavrillo, I.G. Petrov, K.I. Hirayama, M. Mellor, P. Tryde and K.D. Vaudrey (1981) Standardized testing methods for measuring mechanical properties of ice. *Cold Regions Science and Technology*, **4**: 245-253.

Sinha, N.K. (1984) Uniaxial compressive strength of first-year and multi-year sea ice. *Canadian Journal of Civil Engineering*, **11**: 82-91.

Sinha, N.K. (1985) Confined strength and deformation of second-year columnar-grained sea ice in Mould Bay. *Proceedings of the Fourth International Symposium on Offshore Mechanics and Arctic Engineering, 17-21 February, Dallas, Texas.* American Society of Mechanical Engineers, Vol. 2, pp. 209-219.

Sinha, N.K. and R.M.W. Frederking (1979) Effect of system stiffness on strength of ice. *Proceedings of the 5th International Conference on Port and Ocean Engineering Under Arctic Conditions (POAC '79), 13-19 August, Trondheim, Norway.* Vol. 1, pp. 708-717.

Timco, G.W. and R.M.W. Frederking (1983) Confined compressive strength of sea ice. *Proceedings of the 7th International Conference on Port and Ocean Engineering Under Arctic Conditions (POAC '83), 5-9 April, Helsinki, Finland.* Vol. 1, pp. 243-253.

Traetteberg, A., L.W. Gold and R. Frederking (1975) The strain rate and temperature dependence of Young's modulus of ice. *Proceedings of the 3rd International Symposium on Ice Problems, 18-21 August, Hanover, New Hampshire.* International Association of Hydraulic Research, Committee on Ice Problems, pp. 449-486.

Tucker, W.B., A.J. Gow and J.A. Richter (1984) On small-scale horizontal variations of salinity in first-year sea ice. *Journal of Geophysical Research*, **89**(C4): 6505-6514.

Wang, Y.S. (1979a) Sea ice properties. Technical Seminar on Alaskan Beaufort Sea Gravel Island Design, 18 October 1979. Houston, Texas: Exxon Company, U.S.A.

Wang, Y.S. (1979b) Crystallographic studies and strength tests of field ice in the Alaskan Beaufort Sea. *Proceedings of the 5th International Conference on Port and Ocean Engineering under Arctic Conditions (POAC '79), 13-19 August, Trondheim, Norway.* Vol. 1, pp. 651-665.

Wang, Y.S. (1981) Uniaxial compression testing of Arctic sea ice. *Proceedings of the 6th International Conference on Port and Ocean Engineering Under Arctic Conditions (POAC '81), 27-31 July, Quebec, Canada.* Vol. 1, pp. 346-355.

Weeks, W.F. and A.J. Gow (1978) Preferred crystal orientation along margins of the Arctic Ocean. *Journal of Geophysical Research*, **83**(C10): 5105-5121.

Weeks, W.F. and A.J. Gow (1980) Crystal alignment in the fast ice of arctic Alaska. *Journal of Geophysical Research*, **85**(C2): 1137-1146.

APPENDIX A: TEST RESULTS FROM THE UNCONFINED AND CONFINED CONSTANT-STRAIN-RATE COMPRESSION TESTS

The parameters listed for each test are identified in the Index. S.TR1-2-10/0 denotes those compression tests conducted at a strain rate of 10^{-2} s^{-1}, a test temperature of -10°C and a confinement ratio (radial to axial stress) of zero. The sample number P-059-45 gives the location, depth and estimated σ:c angle of the sample; in other words, this sample is from core hole P taken at a depth of 59 cm below the top of the ice sheet at an estimated σ:c angle of 45°.

INDEX

Column number	*Symbol*	*Description*
1	σ_m (lbf/in.^{2})*	Peak stress or strength.
2	ϵ_m (GL) (%)	Strain at σ_m determined by the DCDTs over a gauge length of 14 cm in the unconfined tests *or* by the LVDTs over the full sample length of 25.4 cm in the confined tests.
3	ϵ_m (FS) (%)	Strain at σ_m determined by the extensometer over the full sample length of 25.4 cm in the unconfined tests *or* by the extensometers mounted on the piston shaft triaxial cell in the unconfined tests. The latter measurements have been corrected for load train deformation.
4	t_m (s)	Time to peak stress.
5	σ_e (lbf/in.^{2})*	Time to end of test.
6	ϵ_e (FS) (%)	Full sample strain at end of test.
7	t_e (s)	Time to end of test.
8	E_i (GL) (10^6 lbf/in.^{2})*	Initial tangent modulus determined using strains measured by the DCDTs in the unconfined test *or* by the LVDTs in the confined test.
9	E_o (GL) (10^6 lbf/in.^{2})*	Secant modulus determined using strain measurements from column 2.
10	E_o (FS) (10^6 lbf/in.^{2})*	Secant modulus determined using strain measurement from column 3.
11	S_i (‰)	Sample salinity at test temperature.
12	ϱ (lb/ft^3)*	Sample weight density at test temperature.
13	V_b (‰)	Brine volume at test temperature.
14	V_a (‰)	Air volume at test temperature.
15	n (‰)	Porosity at test temperature.
16	σ_e/σ_m	Ratio of end to peak strain at 5% or 2.5% full sample strain.
17	Ice squareness (in.)*	Sample squareness departure after ends are milled.

Column number	*Symbol*	*Description*
18	End cap squareness (in.)*	Sample squareness departure after end caps are mounted.
19	Shim (in.)*	Amount of steel shim stock inserted between low end of sample and actuator in unconfined test *or* lower piston in confined tests before testing.
20	σ:*c*	Mean angle and standard deviation between the applied load and crystal c-axes.
21	σ:*z*	Mean angle between the applied load and the direction of elongation of the crystals.

* 1 lbf/in.^{2} = 6894.757 Pa; 1 lb/ft^3 = 16.01846 kg/m^3; 1 in. = 2.54 cm.

FILE S.TRI-2-10/0

01	02	03	04	05	06	07	08	09	10	11	12	13	14	15	16	17	18	19	20	21
P-059-45*																				
328	0.042	0.068	0.08	328	0.07	0.08	0.921	0.781	0.482	4.69	56.62	25.5	17.9	43.5		0.072	0.022	0.022	32±15	87
P-126-45																				
754	0.078	0.120	0.13	754	0.12	0.13	1.152	0.967	0.628	3.30	56.84	18.0	12.5	30.5		0.036	0.017	0.017	46	90
P-140-45																				
806	0.077	0.150	0.17	806	0.15	0.17	1.087	1.047	0.537	2.85	56.49	15.5	18.0	33.5		0.056	0.031	0.031	41	88
P-153-45																				
796	0.080	0.110	0.14	796	0.11	0.14	1.065	0.995	0.724	2.81	57.19	15.5	5.8	21.2		0.092	0.022	0.022	28	90

* Sample number.

FILE S.TRI-3-10/0

01	02	03	04	05	06	07	08	09	10	11	12	13	14	15	16	17	18	19	20	21
O-061-45*																				
654	0.110	0.110	1.08	654	0.11	1.08	1.021	0.594	0.594	4.03	56.13	21.8	25.6	47.4		0.018	0.004	0.004	50±13	85
P-097-45																				
385	0.070	0.090	0.74	385	0.09	0.74	0.875	0.550	0.428	3.86	56.55	21.0	18.2	39.2		0.051	0.006	0.006	25±13	80
O-111-45																				
648	0.130	0.170	1.34	648	0.17	1.34	0.940	0.498	0.381	3.84	56.47	20.9	19.5	40.4		0.039	0.054	0.054	50	90
O-136-45																				
653	0.100	0.110	1.20	653	0.11	1.20	1.020	0.653	0.594	3.38	56.29	18.3	22.1	40.4		0.071	0.006	0.006	45	90
O-151-45																				
735	0.120	0.170	1.42	735	0.17	1.42	1.103	0.613	0.432	3.17	56.88	17.3	11.6	28.9		0.043	0.012	0.012	42	84
O-096-45																				
640	0.110	0.140	1.40	640	0.14	1.40	1.000	0.582	0.457	4.36	56.12	23.5	26.2	49.7		0.034	0.020	0.020	48	90
K-060-90																				
716	0.140	0.200	1.16	684	0.22	1.43	0.946	0.511	0.358	4.37	57.05	24.0	10.1	34.1		0.053	0.012	0.012	80	80
H-075-90																				
800	0.120	0.120	1.73	800	0.12	1.73	1.067	0.667	0.667	5.10	56.89	27.9	13.8	41.7		0.046	0.006	0.008	90	80
H-139-90																				
955	0.080	0.130	1.17	955	0.13	1.17	1.287	1.194	0.735	3.50	57.02	19.2	9.6	28.8		0.067	0.003	0.003	89±1	87
K-145-90																				
1333	0.160	0.180	1.73	1333	0.18	1.73	1.297	0.833	0.741	2.90	56.87	15.9	11.4	27.3		0.069	0.012	0.012	90	90
J-077-0																				
917	0.180	0.250	2.19	145	5.00	50.00	1.030	0.509	0.367	4.04	56.84	22.1	13.3	35.4	0.158	0.052	0.022	0.022	5±4	90
J-113-0																				
975	0.110	0.150	1.42	975	0.15	1.42	1.313	0.886	0.650	4.12	57.45	22.8	2.9	25.6		0.037	0.013	0.013	10	88
I-064-0																				
871	0.150	0.190	1.84	139	5.00	50.00	1.101	0.581	0.458	4.37	56.60	23.8	17.9	41.7	0.160	0.075	0.007	0.007	2±6	86
J-169-0																				
1468	0.150	0.210	2.04	1468	0.21	2.04	1.420	0.979	0.669	2.96	57.36	16.3	3.0	19.3		0.028	0.007	0.007	10	90

* Sample number.

FILE S.TRI-5-10/0

01	02	03	04	05	06	07	08	09	10	11	12	13	14	15	16	17	18	19	20	21
P-074-45*																				
87	0.210	0.190	175.0	70	5.00	5000	0.761	0.042	0.046	4.14	57.18	22.8	7.6	30.3	0.800	0.037	0.013	0.013	32±15	87
P-111-45																				
82	0.180	0.180	150.0	63	5.00	5000	0.446	0.046	0.046	3.59	56.72	19.6	14.9	34.5	0.770	0.046	0.012	0.012	35±16	86
O-122-45																				
82	0.130	0.180	160.0	54	5.00	5000	0.480	0.063	0.046	3.47	56.65	18.9	16.0	34.9	0.670	0.025	0.008	0.008	43±1	86
O-165-45																				
93	0.050	0.070	65.00	46	5.00	5000	0.700	0.187	0.013	2.77	56.18	15.0	23.3	38.2	0.490	0.030	0.006	0.006	47±7	83
K-073-90																				
151	0.150	0.160	148.0	68	5.00	5000	0.778	0.101	0.094	3.98	56.88	21.8	12.6	34.4	0.980	0.043	0.009	0.009	80±16	90
H-096-90																				
195	0.120	0.150	150.0	99	5.00	5000	0.770	0.163	0.130	4.49	57.48	24.8	2.8	27.6	0.770	0.042	0.010	0.010	84±17	89
E-098-90																				
218	0.210	0.190	188.0	108	5.00	5000	0.700	0.104	0.115	4.30	56.44	23.3	20.6	43.9	0.860	0.049	0.004	0.004	89±19	86
K-160-90																				
306	0.086	0.150	145.0	87	5.00	5000	0.584	0.356	0.204	2.92	56.97	16.0	9.7	25.7	0.470	0.054	0.001	0.001	86±10	86
I-078-0																				
179	0.140	0.130	135.0	111	5.00	5000	1.080	0.128	0.138	4.72	57.35	26.0	5.3	31.4	0.750	0.032	0.005	0.005	2±17	88
J-100-0																				
166	0.120	0.110	110.0	83	5.00	5000	0.875	0.138	0.151	4.02	56.61	21.9	17.3	39.2	0.660	0.082	0.024	0.024	6±12	90
I-115-0																				
255	0.120	0.130	120.0	129	5.00	5000	1.330	0.213	0.196	4.15	57.33	22.9	5.0	27.9	0.510	0.041	0.007	0.007	2±10	88
I-143-0																				
320	0.170	0.180	160.0	125	5.00	5000	1.313	0.188	0.178	3.29	56.95	18.0	10.5	28.6	0.500	0.048	0.015	0.015	3±8	87

* Sample number.

FILE S.TRI-5-10/0.25

01	02	03	04	05	06	07	08	09	10	11	12	13	14	15	16	17	18	19	20	21
*M-063-45†																				
155		0.320	320.0	133	5.00	5000			0.048	4.44	56.84	24.3	13.8	38.1	0.858	0.036	0.025	0.025	35±14	85
*M-098-45																				
143		0.290	295.0	145	5.00	5000			0.049	4.41	57.10	24.2	9.5	33.7	1.014	0.040	0.013	0.013	32±17	86
*M-128-45																				
152		0.250	250.0	144	5.00	5000			0.061	3.90	57.16	21.4	7.8	29.2	0.947	0.021	0.009	0.009	30±14	90
*M-156-45																				
132		0.120	100.0	116	5.00	5000			0.110	2.97	57.54	16.4	0.2	16.6	0.879	0.025	0.007	0.007	39±14	88
*C-105-90																				
202		0.230	212.0	143	5.00	5000			0.088	3.75	57.27	20.7	5.5	26.2	0.708	0.077	0.033	0.033	82±14	84
*C-171-90																				
171		0.270	260.0	132	5.00	5000			0.063	3.08	58.41				0.772	0.045	0.048	0.048	82±13	87
*H-062-90																				
217		0.230	220.0	147	5.00	5000			0.094	4.46	56.56	24.3	18.7	43.0	0.677	0.057	0.022	0.022	86±12	87
*H-123-90																				
203		0.440	433.0						0.046	3.91	57.17	21.5	7.5	29.0		0.060	0.013	0.012	77±17	86
*A-130-0																				
324		0.220	230.0	249	5.00	5000			0.147	4.33	57.12	23.8	8.8	32.6	0.767	0.059	0.032	0.032	2±7	90
*A-141-0																				
308		0.310	320.0	283	5.00	5000			0.099	4.06	57.20	22.3	7.1	29.5	0.919	0.042	0.037	0.037	0±8	90
*A-103-0																				
274		0.240	270.0	312	5.00	5000			0.114	3.99	56.65	21.7	16.6	38.3	1.139	0.062	0.041	0.041	10±12	90
*B-104-0																				
233	0.340	0.350	333.0	196	2.50	2500	0.903	0.069	0.067	4.79	56.60	26.1	18.6	44.7	0.841	0.013	0.004	0.004	5±7	85
*J-060-0																				
205		0.500	520.0	225	5.00	5000			0.041	3.95	56.40	21.4	20.9	42.3	1.100	0.043	0.009	0.007	3±17	88
*I-130-0																				
394		0.280	310.0	334	5.00	5000			0.141	3.83	55.77	20.5	31.8	52.4	0.848	0.043	0.008	0.008	1±12	90
*J-155-0																				
407		0.280	310.0	286	5.00	5000			0.145	2.94	57.14	16.2	6.8	23.0	0.703	0.044	0.018	0.018	3±10	87

* Strain measurements made by extensometers mounted on piston shaft.
Corrections have been made according to Cox and Richter-Menge (1985).

† Sample number.

FILE S.TRI-3-10/0.25

01	02	03	04	05	06	07	08	09	10	11	12	13	14	15	16	17	18	19	20	21
*M-077-45†																				
914		0.330	3.49	411	5.00	50.00			0.277	4.08	56.53	22.2	18.8	41.0	0.450	0.041	0.029	0.029	42±20	87
*M-114-45																				
970		0.330	3.50	563	5.00	50.00			0.294	4.34	57.29	23.9	6.2	30.1	0.580	0.053	0.020	0.020	35±28	87
*M-169-45																				
997		0.270	2.84	458	5.00	50.00			0.369	2.89	57.16	15.9	6.6	22.4	0.459	0.060	0.027	0.027	41±11	88
*M-144-45																				
1182		0.300	3.12	423	5.00	50.00			0.394	3.16	57.47	17.5	1.5	18.9	0.358	0.018	0.014	0.014	35±15	88
*C-146-90																				
1367		0.320	3.40	485	5.00	50.00			0.427	3.51	56.93	19.2	11.1	30.4	0.355	0.059	0.042	0.042	88±11	85
*E-058-90																				
1172		0.390	4.12	508	5.00	50.00			0.301	4.30	57.02	23.6	10.5	34.1	0.433	0.072	0.035	0.025	87±23	90
E-142-90																				
1870	0.320	0.480	3.12	845	2.50	25.00	0.954	0.584	0.390	3.03	57.16	16.7	6.7	23.4	0.452	0.005	0.005	0.005	86±6	86
*H-111-90																				
1327		0.340	4.20	620	5.00	50.00			0.390	4.26	58.03				0.467	0.044	0.004	0.004	83±18	89
*A-090-0																				
1358		0.390	4.20	826	5.00	50.00			0.348	4.65	57.04	25.5	10.9	36.4	0.608	0.102	0.057	0.057	3±16	86
B-134-0																				
1466	0.430	0.560	5.44	994	5.00	50.00	0.878	0.341	0.262	4.22	57.04	23.2	10.3	33.5	0.687	0.006	0.010	0.010	3±7	87
*I-161-0																				
3127		0.450	5.10	1463	5.00	50.00			0.695	3.13	56.24	16.9	22.7	39.6	0.468	0.060	0.008	0.008	4±6	86
*J-143-0																				
1831		0.580	6.65	1125	5.00	50.00			0.316	3.23	56.96	17.7	10.3	28.0	0.614	0.053	0.005	0.005	5±10	90
A-116-0																				
1753	0.350	0.400	4.00	597	3.64	3640	0.993	0.501	0.438	3.78	56.23	20.4	23.9	44.3	0.341	0.012	0.012	0.012	9±10	90
B-118-0																				
1358	0.290	0.390	2.86	1024	2.50	25.00	0.894	0.468	0.348	4.53	56.41	24.6	21.5	46.1	0.754	0.014	0.008	0.008	8±9	86

* Strain measurements made by extensometers mounted on piston shaft.
Corrections have been made according to Cox and Richter-Menge (1985).

† Sample number.

FILE S.TRI-3-10/0.50

01	02	03	04	05	06	07	08	09	10	11	12	13	14	15	16	17	18	19	20	21
D-057-45*																				
1457	0.340		3.15	1249	2.50	25.00	0.867	0.429		4.08	57.04	22.4	10.2	32.6	0.857	0.005	0.017	0.017	20+17	88
D-083-45																				
1362	0.260		2.54	927	2.50	25.00	1.072	0.524		3.79	57.12	20.8	8.7	29.5	0.681	0.005	0.027	0.010	21+18	86
D-108-45																				
1855	0.560		5.40	1684	2.50	25.00	1.330	0.337		3.95	56.79	21.6	14.3	35.9	0.908	0.004	0.006	0.006	15+18	90
D-135-45																				
1816	0.330		3.05	1419	2.50	25.00	1.067	0.550		3.41	56.79	18.6	13.7	32.3	0.781	0.005	0.013	0.013	26+14	88
K-094-90																				
2138	0.360		3.54	1230	2.50	25.00	1.097	0.594		3.56	56.91	19.5	11.7	31.2	0.575	0.003	0.003	0.003	90+19	86
K-107-90																				
2232	0.350		3.45	1287	2.50	25.00	1.217	0.638		3.93	56.97	21.5	11.1	32.6	0.577	0.002	0.008	0.008	88+10	86
K-119-90																				
2232	0.350		3.38	1135	2.50	25.00	1.237	0.638		3.67	56.91	20.1	11.8	31.9	0.509	0.003	0.012	0.012	86+11	88
K-132-90																				
2308	0.340		3.24	1211	2.50	25.00	1.286	0.679		3.12	56.85	17.1	12.3	29.3	0.525	0.003	0.010	0.010	87+13	89
G-065-0																				
2801	0.360		3.48	1816	1.90	18.92	1.100	0.578		3.43	56.59	18.7	13.7	32.4		0.003	0.008	0.003	9+7	87
L-075-0																				
2535	0.490		4.76	2119	2.50	25.00	1.252	0.517		3.24	57.04	17.8	9.2	26.9	0.836	0.004	0.002	0.002	5+10	88
G-109-0																				
1551	0.390		3.76	1097	2.50	25.00	0.942	0.398		3.99	56.79	21.8	14.4	36.2	0.707	0.004	0.000	0.000	10+18	85
L-142-0																				
3209	0.850		8.60	2573	2.50	25.00	1.329	0.378		2.91	56.60	15.8	16.3	32.2	0.802	0.005	0.007	0.002	4+8	86

* Sample number.

FILE S.TRI-5-10/0.50

01	02	03	04	05	06	07	08	09	10	11	12	13	14	15	16	17	18	19	20	21
U-92-45*																				
191	0.340		335.0	140	2.50	2500	0.644	0.056		3.56	56.04	19.2	26.9	46.0	0.733	0.006	0.004	0.000	50+15	88
S-106-45																				
				193	2.50	2500	0.829			3.87	55.88	20.8	30.5	51.3		0.000	0.015	0.015	34+19	88
U-121-45																				
174	0.290		285.0	148	2.50	2500	0.646	0.060		3.71	56.62	20.2	17.3	37.5	0.851	0.003	0.008	0.008	50+6	90
S-147-45																				
112	0.200		205.0	110	2.50	2500	0.594	0.056		4.03	54.50	21.1	54.5	75.6	0.982	0.005	0.007	0.007	42+12	87
E-083-90																				
440	0.350		350.0	307	2.50	2500	1.261	0.126		4.13	57.04	22.7	10.2	32.9	0.796	0.006	0.014	0.014	88+11	87
E-112-90																				
454	0.180		185.0	321	2.50	2500	0.751	0.252		3.85	56.85	21.1	13.1	34.2	0.408	0.005	0.007	0.007	82+5	82
E-128-90																				
492	0.240		235.0	321	2.50	2500	0.897	0.206		3.62	56.85	19.8	12.9	32.7	0.478	0.004	0.012	0.012	89+9	85
N-153-90																				
643	0.200		200.0	288	2.50	2500	0.887	0.322		2.81	56.92	15.4	10.8	26.2	0.311	0.005	0.008	0.008	86+10	85
L-058-0																				
363	2.310		2312	361	2.50	2500	0.775	0.016		3.71	56.91	20.3	11.9	32.2	0.995	0.002	0.018	0.018	10+11	88
L-098-0																				
				532	2.50	2500	0.649			3.64	56.85	19.9	12.9	32.8		0.006	0.020	0.020	3+10	88
G-124-0																				
274	0.320		320.0	263	2.50	2500	0.773	0.086		3.85	56.91	21.1	12.1	33.1	0.960	0.007	0.024	0.024	5+8	82
L-155-0																				
660	0.760		750.0	643	2.50	2500	1.164	0.087		3.18	56.66	17.3	15.6	32.9	0.974	0.006	0.007	0.007	1+11	89

* Sample number.

FILE S.TRI-3-10/0.75

01	02	03	04	05	06	07	08	09	10	11	12	13	14	15	16	17	18	19	20	21
O-094-45†																				
3474	1.530		15.04	3364	2.50	25.00	1.408	0.227		4.07	56.79	22.2	14.5	36.7	0.968	0.003	0.006	0.006	[illegible]	[illegible]
T-124-45																				
1996	0.370		3.50	1571	2.50	25.00	1.207	0.540		3.56	56.31	19.3	22.5	41.8	0.787	0.002	0.018	0.018	44•13	80
T-137-45																				
1848	0.280		2.50	1423	2.50	25.00	1.193	0.660		3.20	56.31	17.3	22.1	39.4	0.770	0.004	0.006	0.006	45•14	87
T-152-45																				
2199	0.490		3.70	1627	2.50	25.00	1.213	0.550		3.20	56.79	17.5	13.4	30.9	0.740	0.003	0.009	0.009	43•11	87
N-077-90																				
3426	1.050		10.20	2514	2.50	25.00	1.428	0.326		4.08	56.60	22.2	17.7	40.0	0.734	0.003	0.002	0.002	[illegible]	[illegible]
N-108-90																				
4096	1.080		10.60	3918	1.51	13.30	1.457	0.379		3.50	56.75	19.1	14.9	34.0		0.004	0.006	0.006	[illegible]	[illegible]
R-153-90																				
3696	1.730		19.20	3252	2.50	25.00	1.365	0.214		2.57	56.97	14.1	9.4	23.5	0.880	0.009	0.020	0.020	[illegible]	[illegible]
**R-124-90																				
				3238	0.86	8.40	1.497	1.227		3.32	56.56	18.1	17.9	36.0		0.005	0.012	0.012	[illegible]	[illegible]
**R-138-90																				
				3696	0.27	2.70	1.678			2.95	56.81	16.1	13.1	29.2		0.004	0.026	0.026	[illegible]	[illegible]
F-064-0																				
3290	0.750		7.40	2699	2.50	25.00	1.416	0.439		3.37	56.91	18.4	11.5	29.9	0.820	0.005	0.001	0.001	17•11	[illegible]
**O-074-0																				
				4539	1.11	11.00	1.412			4.10	56.66	22.3	16.7	39.0		0.002	0.012	0.012	3•11	90
F-100-0																				
				3844	2.50	25.00	1.510			3.16	56.85	17.3	12.3	29.6		0.004	0.011	0.011	4•7	87
F-127-0																				
				3992	2.45	24.70	1.584			3.64	56.97	19.9	10.7	30.7		0.003	0.014	0.014	5•8	90
**O-95-0																				
				3260	1.16	11.70	1.578	1.216		3.49	56.81	19.1	13.8	32.8		0.004	0.009	0.009	8•10	86
**O-143-0																				
				3268	0.80	7.92		1.180		2.82	56.81	15.4	13.0	28.4		0.007	0.003	0.003	2•10	88

** Test ended early due to limitation in triaxial cell capacity.

† Sample number.

FILE S.TRI-5-10/0.75

01	02	03	04	05	06	07	08	09	10	11	12	13	14	15	16	17	18	19	20	21
T-072-45*																				
				462	2.50	2500	0.924			3.98	56.87	21.8	13.3	35.1		0.005	0.012	0.012	44•14	84
T-094-45																				
				370	2.50	2500	1.014			3.62	56.66	19.7	16.1	35.8		0.004	0.009	0.009	41•12	86
T-109-45																				
				370	2.50	2500	1.013			3.58	56.81	19.6	13.9	33.4		0.003	0.005	0.005	45•15	88
O-120-45																				
				824	2.50	2500	0.960			4.10	57.00	22.5	11.3	33.7		0.004	0.002	0.002	17•17	96
N-061-90																				
601	0.780		770.0	573	2.50	2500	1.803	0.077		3.94	56.81	21.5	14.3	35.8	0.953	0.004	0.018	0.018	83•17	85
N-096-90																				
870	1.040		1035	680	2.50	2500	1.566	0.084		3.66	56.87	20.0	12.9	32.9	0.782	0.003	0.012	0.012	86•14	87
N-123-90																				
1164	0.600		600.0	739	2.50	2500	1.929	0.194		3.58	56.94	19.6	11.7	31.3	0.635	0.004	0.008	0.008	84•14	84
N-166-90																				
1423	0.560		560.0	739	2.50	2500	1.365	0.259		2.93	56.73	16.0	14.2	30.2	0.519	0.003	0.011	0.011	[illegible]	84
F-051-0																				
				831	2.50	2500	1.041			3.96	56.97	21.7	11.1	32.8		0.004	0.024	0.024	10•32	[illegible]
F-083-0																				
				1257	2.50	2500	1.446			3.51	57.22	19.3	6.2	25.5		0.004	0.013	0.013	6•9	84
F-114-0																				
1806	1.660		1645	1349	2.50	2500	1.060	0.083		3.38	57.25	18.6	6.1	24.7	0.973	0.003	0.038	0.038	7•7	96
F-146-0																				
1294	0.980		965.0	1257	2.50	2500	1.450	0.132		3.02	57.10	16.6	7.8	24.4	0.971	0.004	0.004	0.004	4•7	96

* Sample number.

A facsimile catalog card in Library of Congress MARC format is reproduced below.

Richter-Menge, J.A.
Triaxial testing of first-year sea ice / by J.A. Richter-Menge, G.F.N. Cox, N. Perron, G. Durell and H.W. Bosworth. Hanover, N.H.: U.S. Army Cold Regions Research and Engineering Laboratory; Springfield, Va.: available from National Technical Information Service, 1986.
iv, 47 p., illus.; 28 cm. (CRREL Report 86-16.)
Bibliography: p. 32.
1. First-year sea ice. 2. Ice. 3. Ice properties. 4. Mechanical properties. 5. Sea ice. I. United States. Army. Corps of Engineers. II. Cold Regions Research and Engineering Laboratory, Hanover, N.H. III. Series: CRREL Report 86-16.

☆ U.S. GOVERNMENT PRINTING OFFICE: 1987 — 700-050/32,070

END

4-87

DTIC